Subsurface Structure of the East Bay Plain Ground-Water Basin: San Francisco Bay to the Hayward Fault, Alameda County, California

By R.D. Catchings[1], J.W. Borchers[1], M.R. Goldman[1], G. Gandhok[1], D.A. Ponce[1], and C.E. Steedman[1]

Open-File Report 2006-1084

2006

U.S. DEPARTMENT OF THE INTERIOR
U.S. GEOLOGICAL SURVEY

[1] U.S. Geological Survey, 345 Middlefield Rd, Menlo Park, CA 94025

Introduction

The area of California between the San Francisco Bay, San Pablo Bay, Santa Clara Valley, and the Diablo Ranges (East Bay Hills), commonly referred to as the "East Bay", contains the East Bay Plain and Niles Cone ground-water basins (CDWR, 1967*)* (Fig. 1). The area has a population of 1.46 million **(**2003 US Census), largely distributed among several cities, including Alameda, Berkeley, Fremont, Hayward, Newark, Oakland, San Leandro, San Lorenzo, and Union City. Major known tectonic structures in the East Bay area include the Hayward Fault and the Diablo Range to the east and a relatively deep sedimentary basin known as the San Leandro Basin (Marlow et al., 1999; Stanley et al., 2002; Ponce et al., 2003) beneath the eastern part of the bay. Known active faults, such as the Hayward, Calaveras, and San Andreas pose significant earthquake hazards to the region, and these and related faults also affect ground-water flow in the San Francisco (SF) Bay area (Izbicki et al., 2003). Because most of the valley comprising the San Francisco Bay area is covered by Holocene alluvium or water at the surface, our knowledge of the existence and locations of such faults, their potential hazards, and their effects on ground-water flow within the alluvial basins is incomplete.

To better understand the subsurface stratigraphy and structures and their effects on ground-water and earthquake hazards, the U.S. Geological Survey (USGS), in cooperation with the East Bay Municipal Utility District (EBMUD), acquired a series of high-resolution seismic reflection and refraction profiles across the East Bay Plain near San Leandro in June 2002 (Fig. 2). In this report, we present results of the seismic imaging investigations, with emphasis on ground water.

Geology and Tectonics

The San Francisco Bay area is located within a relatively wide segment of the North American-Pacific plate boundary consisting of a number of active right-lateral, strike-slip fault zones, including the San Gregorio, San Andreas, Hayward-Rodgers Creek, Calaveras, and other smaller fault zones (Wallace, 1990; Graymer, 2000). The San Francisco Bay lies within a structural depression between the Diablo Range (East Bay Hills) to the east and the Santa Cruz Mountains to the west (Fig. 1). Within the structural depression, areas between the bay and the mountain ranges are largely covered by Quaternary alluvium (Graymer, 2000). On the eastern side of the bay, the alluvial-covered areas extend about 6 to 15 km from the bay to rock exposures in the Diablo Range. The alluvium and underlying sedimentary units consist largely of late Pleistocene to Holocene unconsolidated marine and continental deposits (Muir, 1993; Figuers, 1998). The marine deposits are largely estuarine mud and salt-marsh deposits, known as Young Bay Mud, Old Bay Mud or the Yerba Buena Mud (Sloan, 1992)), and other minor units (Trask and Rolston, 1951; Ross, 1977; Atwater et al, 1981; Rogers and Figuers, 1991; Sloan, 1992; Ch2M-Hill, Inc., 2000). The continental deposits are mostly coarse-grained stream-channel deposits and finer-grained flood-plain deposits (Sloan, 1992; Koltermann and Gorelick, 1992) that were deposited as coalescing alluvial fans of San Leandro, San Lorenzo, and Alameda Creeks and other drainages along the east side of the San Francisco Bay. Partly consolidated sedimentary rocks and deposits probably underlie the late Pleistocene continental and marine deposits in much of the southern East Bay Plain (Marlow and others, 1999; Izbicki and others, 2003).

In the region, basement rocks beneath the valleys are assumed to be the same as those found in the adjacent mountain ranges, which consist largely of Mesozoic Great

Valley and Franciscan complexes, and overlying Tertiary and younger rocks (Howard, 1979; Graymer, 2000). In the study area, the Great Valley complex is principally composed of dismembered ophiolite and silicic volcanic rocks, which are overlain by Late Jurassic silicic tuff and tuffaceous sandstone, Late Jurassic to Early Cretaceous turbidites, and Late Cretaceous and Paleocene strata (Graymer, 2000). The Franciscan complex is composed of multiple rock types, including graywacke, metagraywacke, metachert, metabasalt, turbidites, sandstone, quartz diorite, and serpentinite (Graymer, 2000). The Tertiary strata consist of various sedimentary and volcanic rocks, which were probably deposited unconformably over the Mesozoic Rocks (Graymer, 2000). Within the East Bay Hills, late Cenozoic faulting and folding (Aydin, 1998; Unruh and Lettis, 1998) have deformed the sequence of rocks**.**

Hydrogeology

Historically, aquifer descriptions were extended into the East Bay Plain from the Niles Cone ground-water basin to the south (Brown and Caldwell, 1986; Maslonkowski, 1988**).** The four aquifers defined in the Niles Cone ground-water basin from shallowest to deepest are the Newark, Centerville, Fremont, and Deep aquifers. Generally, in the East Bay Plain sedimentary deposits that correlate with the Newark aquifer in the Niles Cone ground-water basin lie between depths of 9-40 m (30-130 ft) below land surface (CH2M HILL, 2000). Near the San Francisco Bay these deposits have been intruded by seawater. In the East Bay Plain sedimentary deposits that are correlative with the Centerville and Freemont aquifers in the Niles Cone ground-water basin are discontinuous lenses of sand and gravel interbedded with clays and silts between about 36 and 122 m (120-400 ft) below land surface. Most useable ground water is stored in the Centerville and Fremont equivalent deposits and in the Deep aquifer which lies between about 152 and 198 m (500-650 ft) below land surface in the study area. The aquifer system in the East Bay Plain consists of often discontinuous deposits of alluvial sand and gravel with some aeolian sand, separated by estuarine mud or fine-grained alluvial flood plain deposits.

In the East Bay Plain ground-water basin, the Deep aquifer is thickest and most continuous south of San Leandro (Izbicki et al., 2003). Luhdorff and Scalmannini (2003) proposed that a stratigraphic or structural transition partly restricts hydraulic interconnection within the Deep aquifer between the East Bay Plain and Niles Cone ground-water basins. They identified eight distinct coarse-grained stratigraphic units within the Deep aquifer underlying the southern East Bay Plain and within their transition zone. Sediments comprising the Deep aquifer in the study area may have been deposited further south, in the alluvial fan of Alameda Creek, and moved to the northwest by right-lateral motion on the Hayward Fault **(**Maslonkowski, 1988; Koltermann and Gorelick, 1992).

Considerable hydraulic connection between the two ground-water basins has been demonstrated only in the Deep Aquifer **(**Luhdorff and Scalmannini, 2003**)**. Ground water in sediments overlying the Deep aquifer generally flows from east to west from the Oakland Hills to San Francisco Bay (SF Bay Regional Water Quality Board, 2004; CH2MHill, 2000**).** Ground-water flow in the Deep aquifer may have a northerly component that has not been seen in the shallower aquifer system.

Knowledge of the aquifer system in the study area is principally derived from drillers' reports and associated bore hole geophysical logs collected from production and monitoring wells. Because of the complex depositional environment, where alluvial fan deposits interfinger with estuarine deposits, and because wells are spread widely over the

ground-water basin, it is difficult to correlate stratigraphy from well to well. High-resolution seismic imaging methods, like those presented in this report, combined with well-log data, provide a means to more closely correlate stratigraphic horizons and structural complexity that affect ground-water flow across the East Bay Plain.

Seismic Survey

Data Acquisition

In June 2002, the USGS acquired a ~6-km-long, high-resolution seismic transect from the SF Bay to the Hayward fault (Fig. 1). Most (~4.2 km) of the transect trended along San Lorenzo (SL) Creek, and the remaining segments were acquired along accessible paths toward the Hayward Fault (Fig. 2). For ease of processing the data, we divided the transect into six nearly linear segments or "profiles", here referred to as profiles SL-1 through SL-6. Acquisition parameters are presented in Table 1.

We used a combination of Betsy-Seisgun™ blasts, down-hole explosive blasts, and dropped weights as seismic sources. Betsy Seisgun™ blasts consisted of 400-grain shotgun blanks in 0.3-m-deep holes, and down-hole explosive sources consisted of ~150-g (1/3 lb.) pentolite explosives in 2-m-deep holes. Along paved streets near the Hayward fault, we used an accelerated weight-drop source, borrowed from Lawrence Livermore National Laboratory. The combination of seismic sources was spaced at 5-m increments along the seismic profile, except where cultural features limited their use.

The data were recorded using an array of four Geometrics Strataview™ RX 60 seismographs, each with 60 active channels (240 total active channels), mated to 40-Hz, single-element, Mark Products L-40A™ vertical geophones. The geophones were spaced at 5-m increments along the profile and co-located (1-m separation) with the seismic sources. Shot timing was determined electronically at the seismic source when a hammer, used to trigger the seisgun, electrically closed contact with the Betsy Seisgun™, sending an electrical signal to the seismograph. The weight-drop source similarly triggered the seismographs electronically upon impact with the ground surface. For the explosive source shots, seismographs and seismic sources were manually triggered, and timing was determined from up-hole times at the co-located geophones.

Data were acquired using a shoot-through acquisition technique, whereby recording sensors remained stationary as shots were fired through the actively recording array. Typically, shots were fired through one-half to three-quarters of the active array before the southwestern 60 channels were moved to the northeastern end of the active array. This process of moving the seismic array was utilized for all segments of the profile that were longer than 1200 m. Three seconds of data were recorded for sources generated by the Betsy Seisgun™ and weight-drop, and five seconds of data were recorded for the explosive shots. The data were recorded in SEG-2 format on the hard drive of Geometrics™ seismographs during field acquisition and were later transferred to 4-mm tape in SEG-Y format for long-term storage.

Table 1. Acquisition parameters for Profiles SL-1 though SL-6. Distances are relative to the first and last geophone. Cumulative length does not include recording lapse.

Profile #	Orientation	Length of geophone profile (m)	Length of shot point profile (m)	No. of shots	No. of CDPs	Max fold	Cumulative Length (m) (geophones)
Profile SL1	SW-NE	2833	2799	538	1153	168	2833
Profile SL2	W-E	729	708	148	311	148	3562
Profile SL3	W-E	673	673	130	287	130	4235
Profile SL4	SW-NE	270	260	26	107	26	4505

Profile SL5	SW-NE	284	244	39	95	39	4789
Profile SL6	SW-NE	574	574	115	233	115	5363

Shot-point and Receiver Locations and Theoretical Fold

Prior to acquiring the seismic data, geophone and shot locations were surveyed using a measuring tape. After acquiring the data, geodetic positions of every shot location and every 20th geophone position were determined using either a differential Global Positioning System (GPS) or an Electronic Distance Measurement ((EDM) instrument. Surveyed locations may be accurate to within 0.05 m. Locations of geophones that were not surveyed were interpolated from the surveyed geophone locations.

Lateral variations in the elevations of shot points and receivers may cause inaccuracies when stacking reflection data and when determining velocities if the variations are not included in processing. We have accounted for these elevation variations during data processing but we include profile geometries in Appendices A-G for reference. Graphical displays of the profile geometries are also presented, including plots of shot and geophone elevations, shot and geophone lateral variations, and fold (Figs. 3-8).

Profile SL 1

Profile SL 1 was oriented southwest-northeast, and it extended 2833 m along the southern side of San Lorenzo Creek from the San Francisco Bay to Washington Avenue (Fig. 2). A total of 538 shots were fired, with 43 shot points not utilized due to cultural features. Geophone elevations varied by about 8 m over a distance of about 2833 m **(**Fig. 3a), and the geophone array deviated laterally from a linear array by 89 m (Fig. 3b), which is about a 3% lateral variation relative to profile length. Shot point elevations varied about 7 m along the 2799-m-long shot point array (Fig. 3c) and varied laterally from a linear array by about 88 m (Fig. 3d). For purposes of stacking the reflection data, fold along SL-1 varied with distance along the profile because of changes in geophone placement described above. Maximum fold was greater than 160, decreasing to 1 at the ends of profile SL-1 (Fig. 3e).

Profile SL 2

Profile SL-2 was oriented west to east, and it extended 729 m along the northern side of San Lorenzo Creek from Washington Avenue to Embers Way at the I-880 freeway. Three RX-60 seismographs with 159 active channels were used to record the data. A total of 148 shots were fired, with five shot points not utilized due to cultural features. Geophone elevation varied by about 4 m along the 729-m-long profile (Fig. 4a), and the geophone array varied laterally by about 58 m relative to a linear array of the shot points, an approximately 8% lateral variation relative to profile length (Fig. 4b). Shot point elevations varied by about 4 m along the 708-m-long shot point array (Fig. 4c), and shot points varied laterally from a linear array by about 44 m (Fig. 4d), a 6% variation. Theoretical stacking fold along SL-2 varied smoothly along the profile because of the stationary recording array, with a maximum fold of 148 near the center, decreasing to one at the ends of the profile (Fig. 4e).

Profile SL 3

Profile SL 3 was oriented west to east, and it extended 673 m along the northern side of San Lorenzo Creek from the I-880-freeway overpass at Hesperian Boulevard to

the Southern Pacific railroad tracks at Lewelling Boulevard. Three RX-60 seismographs with 144 active channels were used to record the data. A total of 130 shots were fired, with 14 shot points were not utilized due to cultural features. Geophone elevation varied across the 673-m-long profile by about 2.5 m (Fig. 5a), and the geophone array varied from a linear array by about 47 m (Fig. 5b), an approximate 7% lateral variation relative to the profile length. Shot point elevations also varied by about 2.5 m along the 673-m-long shot point array (Fig. 5c), with shot points varying laterally relative to a linear array by about 46 m (Fig. 5d). Fold along SL-3 varied smoothly along the profile because of the stationary recording array. Maximum fold was 130 near the center of the profile, decreasing to one at the ends of the profile (Fig. 5e).

Profile SL 4

Profile SL 4 was oriented southwest-northeast, originating at the Southern Pacific railroad tracks (north of Lewelling Blvd.) and extending northeast 270 m across the athletic fields of San Lorenzo High School. One RX-60 seismograph with 55 live channels was used to record the data. A total of 26 shots were fired, with 29 shot points not utilized within the confines of the school's football field. Geophone elevation varied across the 270-m-long survey by about 1.6 m (Fig. 6a), and the geophone array varied laterally relative to a linear array by about 1 m (Fig. 6b), approximately a 0.4% lateral variation relative to the profile length. Shot point elevations also varied about 2 m along the 260-m-long shot point array (Fig. 6c), with a lateral variation relative to a linear array of about 1.2 m (Fig. 6d). Fold along SL-4 varied considerably across the profile because of the missing shot points across the football field (Fig. 6e). A maximum fold of 26 was obtained near the middle of the profile. However, much of the western half of the profile had a fold of only three due to the unused shot points. Fold decreased to one at the ends of the profile.

Profile SL 5

Profile SL 5 was oriented southwest to northeast (Fig. 2). The profile originated at Ashland Avenue and the southwest entrance to Edendale Park, and it extended 284 m northeast to the northeastern corner of Edendale Park. One RX-60 seismograph with 58 active channels was used to record the data. A total of 39 shots were fired, with 19 shot points not utilized due to cultural features such as sprinklers and a children's playground. Geophone elevation varied by about 1.3 m along the 284-m-long profile (Fig. 7a), with the geophone array varying laterally from a linear array by about 2.1 m (Fig. 7b), an approximately 0.7% lateral variation relative to the profile length. Shot point elevations also varied about 1.3 m along the 244-m-long shot point array (Fig. 7c), with lateral variation relative to a linear array of about 2 m (Fig. 7d) or about 0.8%. Fold along SL-5 varied smoothly across the profile because of the stationary recording array. Maximum fold was 39 near the center of the profile, decreasing to one at the ends of the profile **(Fig. 7e**).

Profile SL 6

Profile SL 6 was oriented southwest to northeast (Fig. 2). The profile extended 574 m from near the corner of E-14th Street and 163rd Avenue (on the northwestern side of 163rd Avenue) to Liberty Street at the I-580 freeway. Two RX-60 seismographs with 117 active channels were used to record the data. A total of 115 weight-drop sources were used, with two shot points not utilized due to cultural features. Geophone elevation varied by about 11 m across the 574-m-long profile (Fig. 8a), with the geophone array

varying laterally relative to a linear array by about 2.5 m (Fig. 8b), approximately a 0.4% lateral variation relative to profile length. Shot point elevations also varied by about 11 m along the 574-m-long shot point array (Fig. 8c), and the shot point array varied relative to a linear array by about 4.9 m (Fig. 8d). Fold along SL-6 varied smoothly along the profile because of the stationary recording array. Maximum fold was 115 near the center of the array, decreasing to one at the ends of the profile (Fig. 8e).

Seismic Imaging Method

Because of the shoot-through acquisition method, we developed reflection and refraction images from the same data. Individual profiles were analyzed separately, but we present them here as a composite image so that the images can be seen in the context of the entire seismic profile. However, we describe specifics of data processing and inversion for each profile so that possible anomalies and artifacts can be pointed out.

Data Analysis

First-arrival refractions from usable seismograms were used to develop a P-wave tomographic velocity model of the shallow subsurface along each seismic profile. We used a modified version of an algorithm by Hole (1992), whereby we parameterize the starting model into 5-m by 5-m vertical and horizontal grids. As a check on the validity of the model, we utilized multiple starting models, all of which yielded similar final models. Velocities were measured at depths ranging from about 3 m below the ground surface (bgs) to maximum depths of about 120 m bgs. The depth of velocity imaging was largely determined by the maximum distance that clear first arrivals could be observed on the seismic records. Because of the noisy urban environment, clear first arrivals were typically observed to lateral distances of about 600 m or less from the source. For greater depths, velocities needed for seismic reflection stacking were determined using semblance, parabolic methods, and apriori knowledge of the local geology, derived by combining borehole and empirical data. We also used the inversion-derived velocities to convert the reflection time images to depth images and to migrate the seismic reflection images.

Seismic Refraction Images

Composite Velocity Image

Near-surface velocities along profile SL-1 vary from 900 m/s near the northeastern end of the profile to about 1400 m/s at the southwestern end of the profile (Fig. 9). At approximately 100 m depth, velocities range from 1800 m/s on the southwestern end of the profile to about 2000 m/s on the northeastern end. Near-surface velocities along SL-1 are generally greater near the bay (southwest end of the profile) than those farther to the northeast. Because P-wave velocities in relatively thick sequences of unconsolidated and saturated sediments are typically at least 1500 m/s (Nur, 1982; Schon, 1996), we can use the 1500 m/s velocity contour (white contour, Fig. 9) to infer lateral variations in the top of continuously water-saturated sediments along the profile. However, because the model is a smoothed average over vertical and lateral distances of about 10 to 15 m (2 to 3 grids), the 1500 m/s velocity contour probably infers relative depth variations, not the exact depths of continuously saturated sediments. Another factor that may influence the velocity variations is the presence of faults, which can result in shallower depths to the 1500 m/s velocity contour in saturated rocks

(Mooney and Ginzburg, 1986). Thus, some of the vertical variation in the depth of the 1500 m/s velocity contour may be related to faulting and fracturing.

On the basis of variations in the depth of the 1500 m/s velocity contour across the East Bay Plain, we suggest that, generally, the water table is shallowest near the San Francisco Bay and deepens toward the Hayward Fault. However, there are several local variations in the depth of the 1500 m/s contour that suggest the depth to the water table changes or shallow-depth sediments have been disrupted by faulting. Along profile SL-1, two distinct zones with relatively greater depths to the 1500 m/s velocity contour are centered near meters 250 and 2300 of the seismic profile. These zones are also seen as anomalies in the seismic reflection images, and as discussed below, the zones may correlate with significant shallow-depth faulting.

Velocities along profile SL-2 vary from 800 m/s at the surface to 1900 m/s at a depth of about 100 m (Fig. 9). Across much of the seismic profile, the depth to the 1500 m/s velocity contour does not vary significantly. However, there is appreciable variation in the depth of the 1500 m/s contour near the ends of the seismic profile. We cannot rule out possible edge effects, resulting from too few raypaths at depth near the ends of the array, as causing the depth variations near the ends of the profile. However, as discussed below, we conclude that the apparent variation in the depth of the 1500 m/s velocity contour near the northeast end of the profile is probably due to lateral changes in structure and/or composition. Generally, near-surface velocities are lower along profile SL-2 relative to those along profile SL-1, particularly along the northeastern section of the profile. Lateral complexities in the higher-velocity (deeper) strata (> 1500 m/s) are probably related to lateral variations in composition or structure along the profile.

Near-surface velocities along profile SL-3 vary from 800 m/s on the southwest end of the profile to 1100 m/s on the northeast end. At depths of about 80 m, maximum velocities are about 1850 m/s along the profile (Fig. 9). The 1500 m/s velocity contour, which is outlined in white on the velocity image, varies from about 20 m to about 35 m deep along the seismic profile, with the greatest depth occurring near the northeast end of the profile. The greater depths to the 1500 m/s contour near the northeast end of the profile may be related to raypath edge effects, but we suggest that the greater depths are related to structural or compositional variations based on two observations. First, the 1500 m/s velocity contour deepens more than 100 m southwest from the northeast end of profile SL-3. Ray-path edge effects are unlikely to occur that far from the end of the profile, especially at shallow depths. Second, the 1500 m/s contour is deep at both the northeastern end of profile SL-3 and the southwestern end of profile SL-4. Higher velocities (>1700 m/s) also show appreciable lateral variation, suggesting considerable structural or compositional variation at depth.

Due to the relatively short length of profile SL-4, we obtained velocities to maximum depths of only 40 m. Near-surface velocities along profile SL-4 vary from 800 m/s to 1100 m/s (Fig. 9), with the highest near-surface velocities near meter 100 of the seismic profile. The relatively higher near-surface velocities are likely due to soils with high water content on the San Lorenzo High School football field, which recently had been seeded and was being watered during data acquisition. From the near surface to about 40 m below land surface, velocities increase to about 2000 m/s, which are high relative to those along profiles SL-1 through SL-3. For velocities greater than about 1200 m/s, the velocity contours largely dip to the southwest, suggesting more structural or compositional complexity toward the southwest. In particular, the 1500 m/s velocity contour dips southwestward, and it largely coincides with the 1500 m/s velocity contour near the northeastern end of profile SL-3. These similar variations in velocity near the

adjoining ends of the two profiles suggest structural or compositional anomalies in this vicinity of the East Bay Plain.

The relatively short length of profile SL-5 (~300 m) limited our velocity measurements to maximum depths less than 50 m along the profile. Near-surface velocities range from 700 to 900 m/s, with minor lateral variation in velocity or depth of velocity contours (Fig. 9). The velocity gradient in the upper 20 m is high, reaching 1500 m/s at about 18 m and about 2000 m/s at depths less than 40 m. Low-velocity sediments (< 1500 m/s) do not vary appreciably in depth along the profile, but higher-velocity (> 1500 m/s) sediments vary considerably in depth along the profile, with the greatest depths near the southwestern end of the profile. The appreciable lateral variations in velocity below the 1500 m/s contour may suggest structural complexity below depths of about 20 m.

The approximately 575-m length of profile SL-6 allowed us to determine velocities to a maximum depth of approximately 75 m (Fig. 9**)**. Near-surface velocities vary from about 800 to about to 1100 m/s in the upper 10 m, with higher near-surface velocities near meter 150 and between meters 400 and 450. High-velocity gradients in the upper 25 m are prominent, with maximum velocities of about 1800 m/s. The thickness of near-surface, low-velocity (< 1800 m/s) deposits does not vary significantly along the profile, although there is slightly greater thickness to the southwest. However, the depth of higher-velocity deposits (>1800 m/s) varies appreciably along the profile; high-velocity deposits are significantly deeper on the southwest end of the profile.

Collectively, the velocity profiles suggest that low-velocity, unconsolidated, unsaturated sediments (< 1500 m/s) are relatively thin (< 5 m) near the San Francisco Bay, and they deepen (~40 m maximum) toward the center of the East Bay Plain (west of Washington Avenue). From near Washington Avenue eastward, the low-velocity sediments decrease in thickness toward the East Bay Hills to about 15 m or less. Velocities of 1500 m/s and higher follow a similar trend across the East Bay Plain, with lateral variations in velocity occurring abruptly. Such large changes in the velocity structure, occurring over relatively short distances, probably indicate tectonic disruption of sediments that may affect the ground-water-flow system.

Seismic Reflection Data Processing

In seismic-reflection data processing, we followed procedures similar to those outlined by Brouwer and Helbig (1998). Processing steps included geometry installation, independent trace editing, timing corrections, elevation static corrections, AGC, bandpass filtering, F-K filtering (or surgical muting), velocity analysis (from refractions, semblence, and borehole-velocity measurements), NMO correction, stretch muting, common-depth-point (CDP) stacking, post-stack AGC, post-stack bandpass filtering, and post-stack deconvolution. Principal parameters used in processing are shown in Table 2. For migrated images, we applied pre-stack Kirchoff depth migration after velocity analysis.

In trace editing, noisy traces (due to cultural noises) or redundant traces (due to geometry) were removed from the shot gathers before stacking or migrating. Elevation statics, migration, and velocity analysis were accomplished, in part, using the tomographic velocity model from each profile. For velocities at depths in excess of those determined by the tomography velocity model, we used parabolic methods, and we inferred velocities based on lithologic logs from nearby wells and velocity-depth (pressure) relations (Carmichael, 1989).

Table 2. Processing parameters for the San Leandro seismic profiles.

Parameter	SL-1	SL-2	SL-3
CDP Spacing	2.3 – 2.5 m	1.7 – 2.5 m	2.3 – 2.5 m
AGC			
Prestack	500 ms	500 ms	500 ms
Poststack	100 ms	100 ms	100 ms
Bandpass Filtering			
Notch	60, 120 Hz	60,120 Hz	60, 120 Hz
Prestack	15-30-400-800 Hz	15-30-400-800 Hz	15-30-200-400 Hz
Poststack Low	15-30-400-800 Hz	15-30-400-800 Hz	15-30-400-800 Hz
Poststack High	50-100-200-400 Hz	50-100-200-400 Hz	50-100-200-400 Hz
FK Filter (min-max veloc, min-max freq., k-space restrict.)	90m/s,800m/s,1Hz, 600Hz 50%	90m/s,800m/s,1Hz, 600Hz 50%	90m/s,800m/s,1Hz, 600Hz 50%
Migration (freq., aperture, angle)	400Hz, 400m, 30deg	400Hz, 200m ,60deg	400Hz, 200m, 30deg

Parameter	SL-4	SL-5	SL-6
CDP Spacing	2.4 – 2.6 m	2.4 – 2.6 m	2.4 – 2.8 m
AGC			
Prestack	500 ms	500 ms	500ms
Poststack	100 ms	100 ms	100ms
Bandpass Filtering			
Notch	27 Hz	27 Hz	27 Hz
Prestack	15-30-400-800 Hz	15-30-400-800 Hz	15-30-400-800 Hz
Poststack Low	15-30-400-800 Hz	15-30-400-800 Hz	15-30-400-800 Hz
Poststack High	50-100-200-400 Hz	50-100-200-400 Hz	50-100-200-400 Hz
FK Filter (min-max veloc, min-max freq., k-space restrict.)	90m/s,800m/s,1Hz, 600Hz 50%	90m/s,800m/s,1Hz, 600Hz 50%	90m/s,800m/s,1Hz, 600 Hz 50%
Migration(freq., aperture, angle)	400Hz, 200m, 30deg	400Hz, 200m, 30deg	400Hz, 100m, 30deg

Seismic Reflection Images

We developed seismic reflection images along each of the six profiles by stacking secondary arrivals from the same shot gathers used to obtain the velocity image. We present composite seismic reflection images of the East Bay Plain transect with relatively low frequencies (30-60-200-400 Hz; Figs. 10 and 17a), relatively high frequencies (50-100-200-400 Hz; Fig. 11), and intermediate frequencies (25-50-400-800 Hz; Fig. 17b). The lower-frequency stacks image to greater depths, and the higher-frequency stacks more clearly resolve the upper few hundred meters of the subsurface. Thus, some of the images show structure at depths of 1500 m or more, and other images show details of the shallow (upper few hundred meters) subsurface.

Reflection Images: Profiles SL-1 Through SL-6

Numerous sub-horizontal reflections are imaged in the upper few hundred meters at relatively low frequencies (30-60-200-400 Hz) on the SL profiles (Fig. 10). These reflections correlate with sequences of sediments (sand, clay, and gravel) known to underlie the East Bay Plain (Izbicki et al., 2003), but at relatively low frequencies, thin

layers may be averaged and represented on reflection images as a single reflector. Furthermore, the reflection images do not discriminate between individual layers of coarse or fine-grained sediment; instead, such layers are probably indicated as groups or sequences of sediments containing mixed textures. The lateral continuity of the more prominent reflectors suggests that the same or similar stratigraphic layers or groups of layers persist across the East Bay Plain from the bay to the Hayward fault, although these layers may differ laterally in content, such as grain size, degree of consolidation, and amount of tectonic disruption. Vertical offsets of stratigraphic layers and folding of layers in the reflection images suggest that the layers are disrupted at multiple locations along the SL profiles. Apparent disruptions in the stratigraphic layers occur along profile SL-1 between meters 200-400 and meters 1900-2800 and along much of profile SL-6. At these locations, the reflection image is distorted by diffractive energy. Such disruption is often associated with faults, but might result from the non-linear geometry of the seismic array in specific locations. Several observations argue against non-linear geometric distortion. First, the location and degree of disruption of the layers do not coincide with the location and degree of curvature of the seismic profile (see Figs. 2-8). Second, vertical offsets in the sedimentary layers persist beyond the areas of curvature of the seismic profile. Third, there are similar disruptions in the sedimentary layers in areas where the seismic array is linear. Fourth, the most disrupted reflectors coincide with zones of relatively low velocities; fault zones and low P-wave velocities have been well documented elsewhere (Mooney and Ginzburg, 1986; Catchings, 1999; Catchings et al., 2002). On the basis of these observations, we suggest that the disrupted layers and the corresponding degraded reflection images result from vertical and horizontal offsets (faulting) and fracturing. The layered strata are disrupted in all depth ranges from the very near surface to at least the base of the layered strata, as inferred by the reflectivity pattern of the deeper seismic images.

The thickness of layered strata is highly variable along the seismic transect. For example, within 1300 m of the San Francisco Bay (profile SL-1), strong reflections persist to depths in excess of 800 m, which is the greatest depth of such reflections observed along the seismic transect. Northeast of meter 1300 of profile SL-1, the deep (800 m) reflectors abruptly terminate, and from meter 1300 to about meter 1900 of profile SL-1, the sub-horizontal reflectors become progressively shallower (from ~800 to about 400 m deep) along an apparent series of faults. Because these reflectors do not dip significantly to the southwest, they probably were not deposited in an existing basin but were vertically offset after deposition. At depths of about 400 m and less, some of the more prominent reflectors are offset vertically at multiple locations along the seismic transect.

Rocks underlying the layered strata are largely non-reflective, with depth to the top of the non-reflective rocks ranging from about 200 to 800 m along the East Bay Plain seismic transect. These non-reflective rocks are probably Franciscan basement rocks, but on the basis of reflectivity alone, we cannot be certain that some of the non-reflective rocks below 800m are not sediments. However, if the rocks below about 800 m depth are sediments, they are not sub-horizontally layered and probably dip at high angles to account for the lack of reflectivity.

Higher-Frequency Stacks

To provide more details of the upper 500 m along the seismic transect, we developed a higher-frequency (50-100-200-400 Hz) reflection image (Fig. 11). Because the frequency of the seismic wave determines, in part, which layers (minimum thickness) are imaged, higher-frequency seismic data can image thinner layers when all other

parameters are the same. Whereas the lower-frequency seismic sections image a series of thin layers as a single reflector, multiple thin layers can be resolved with the higher-frequency data. The general formula (Dobrin and Savit, 1988) used to determine the minimum layer thickness needed to generate reflections is the one-quarter-wavelength criteria, where wavelength is:

$\lambda = v/f$, *where* v = *velocity (m/s),* λ = *wavelength (m), and* f = *frequency (Hz*): and the radial width or length of the reflector is related to the Fresnel zone (W*):*

$\omega = v/4\ (\mathrm{sqrt}(t/f))$, *where t is time (sec), v=velocity (m/s):*

Only stratigraphic layers that are about one-fourth of λ and ω will likely generate reflections seen in figure 11. The minimum thickness of the reflectors varies with velocity, but assuming dominant frequencies of 100 Hz and average velocities of 1500 m/s, as determined in the shallow subsurface along this transect, the shallow reflectors imaged in figure 11 are at least 4 m thick and 5 m long. Thus, layers thinner than about 4 m and those with radii less than 5 m cannot be resolved with our data. Both the high- and low-frequency stacks show similar strata, but the high-frequency stack provides more detail, from which we correlate well logs and known stratigraphy.

Well Logs

Several wells with lithologic and/or electric borehole geophysical logs are located within 1 km of the seismic transect (Fig. 12). Most of these wells are several hundred meters from the seismic profile. To compare the borehole geophysical logs with the seismic images, we projected the wells perpendicularly onto the seismic profile (Figs. 12 and 13). The stratigraphy should be generally consistent over distances of several hundred meters, although the exact stratigraphic sequence and depths to stratigraphic horizons beneath the seismic profile may differ somewhat from those determined in the wells because the wells and the seismic transect are not co-located.

We identified 27 deep wells (>400 ft deep) along the seismic transect with available geophysical and/or lithologic logs. We plotted five geophysical logs from wells close to the seismic profile on the seismic sections. Wells 3S3W-14K12, 3S3W-13M4, and 3S3W-13D7 project perpendicularly to profile SL-1 at approximately meters 570, 1010, and 1435, respectively, of the profile. Well 3S2W-7E1 projects to profile SL-2 at about meter 660, and well 3S2W-7G12 projects to profile SL-4 at about meter 145. Both spontaneous potential and resistivity logs are available for each well; however, for display purposes, we include only the short-normal resistivity logs on the seismic sections. We plotted seven lithologic logs from wells close to the seismic profile on the seismic sections. Wells 3S3W-14F1, 3S3W-14K2, 3S3W-14G2, 3S3W14J2, 3S3W-12R1, project perpendicularly to profile SL-1 at meters 485, 525, 640, 840, 2570, respectively, of the profile. Well 3S3W-12H1 projects perpendicularly to the trend of the seismic profile at about meter 425 of profile SL-2, and well 3S2W-6R2 projects perpendicularly to profile SL-5 at about meter 175.

The projected wells are not uniformly spaced along the seismic transect. There is only one nearby well along profile SL-5 and no wells near profile SL-6, making it more ambiguous to correlate known lithologies and these seismic images. Along profiles SL-1 through SL-4, we correlate the seismic images with well-log data and infer lateral variations in sedimentary sequences that include major aquifers (Fig. 13). However, we emphasize that our interpretation is non-unique, particularly between the various seismic profiles and along profile SL-4, where the seismic image is degraded due to missing shot points. On the basis of our correlations, we suggest that the sedimentary sequences that contain the aquifer materials in some places are continuous across the East Bay Plain, but

some layers are disrupted (vertically offset) in multiple locations. Although these sedimentary sequences appear continuous across much of the East Bay Plain, we emphasize that their compositions (grain size, lithology, etc.) may vary significantly along the seismic profile. These sedimentary sequences also vary in depth, but the general trend is for sequences to shallow to the northeast. Sub-horizontal reflectors below the Deep Aquifer along profiles SL-1 and SL-6 suggest that additional thick sedimentary sequences underlie the Deep aquifer, but the water-yielding potential of these sediments cannot be obtained from the seismic data. The deeper sedimentary sequences appear to be of limited lateral extent and do not extend across the entire East Bay Plain. The termination of sub-horizontal reflections along profile SL-6 suggests that most sedimentary sequences containing aquifers terminate west of the surface trace of the Hayward fault.

Gravity Data and Models

For this investigation, D.A. Ponce acquired gravity data along the East Bay Plain seismic transect (Table 3) that compliment a regional gravity data set published by Ponce (2001). Along the East Bay Plain seismic transect, gravity measurements were made every 40 m (every 8th seismic shot point) to help constrain the seismic observations (Fig. 14). The raw data were reduced to provide the Bouguer (complete and simple) anomaly, which ranges from about –2.6 mgal near the Bay to about 20.5 mgal near the Hayward fault. The overall gravity field increases to the northeast along the seismic transect, but there are local anomalies superimposed on the regional trend, suggesting structural variations in the upper few kilometers.

We developed a 2-D gravity model along the East Bay seismic transect (Figs. 15), and we compare our model with another gravity model (Ponce et al., 2003) adjacent to the East Bay Plain seismic transect (Figs. 14 and 16). We used densities similar to those of Ponce et al. (2003**),** with Franciscan basement, the San Leandro gabbro, and the basin sediments having densities of 2.67 g/cm^3, 2.48 g/cm^3, and 2.2 g/cm^3, respectively. Our model was developed using depths to basement inferred by the deepest sub-horizontal reflectors seen on the seismic transect (Fig. 16). Along the seismic transect, our gravity model assumes that variations in the gravity field are largely an indication of changes in the depth to Franciscan basement. Although lateral variations in the sedimentary section likely contribute to small anomalies in the gravity field, the largest anomalies in the gravity field are likely due to variations in the depth of basement rocks. Thus, our simplified model is probably indicative of the relative variation in the depth of basement rocks along the East Bay Plain seismic profile.

Our gravity models suggests that Franciscan basement is about 900 m deep from the eastern shore of the SF Bay to about meter 1500 of the seismic profile, where it abruptly rises to about 525 m depth. From about meter 1500 to about meter 2200, basement rises along a series of steps to about 400 m depth. Along the remainder of the profile, basement varies in depth between about 200 and 400 m, except at the northeastern end of the profile, where basement sharply rises to within 50 m of the surface. Generally, the combined seismic/gravity model suggests a large vertical change in depth of basement near the bay, a small basin near the center of the transect, and a sharp rise in basement at the northeast end of the profile (Fig. 15). Our gravity model (based on seismic reflection images) is also consistent with basement depths modeled by Ponce et al. (2003) along an adjacent transect (Fig. 16), suggesting that the seismically imaged variations in basement structure are accurate.

Table 3. Principal facts of gravity stations along the SL seismic transect. Latitudes and longitudes are based on the North American Datum 1927 (NAD27). CBA, complete Bouguer anomaly; Elev., elevation; FAA, free–air anomaly; ISO, isostatic anomaly; OG, observed gravity; SBA, simple Bouguer anomaly; TC, terrain correction.

Station Name	Location Lat (Degrees	Location Lon Degrees	Elev Feet	Observed Gravity mGal	FAA mGal	SBA mGal	TC Inner mGal	TC Outer mGal	CBA mGal	ISO mGal
02SF3002	37 41.08	122 7.71	31.7	979954.48	-7.01	-8.09	0.28	1.08	-7.02	-7.88
02SF3018	37 41.10	122 7.67	34.3	979954.69	-6.59	-7.76	0.18	0.98	-6.78	-7.61
02SF3030	37 41.12	122 7.63	37.2	979954.58	-6.45	-7.72	0.18	0.99	-6.75	-7.55
02SF3050	37 41.12	122 7.57	34.7	979954.99	-6.28	-7.46	0.18	1	-6.48	-7.24
02SF3074	37 41.15	122 7.50	36.8	979955.19	-5.92	-7.18	0.18	1	-6.19	-6.91
02SF3090	37 41.16	122 7.45	37.7	979955.35	-5.69	-6.98	0.3	1.12	-5.87	-6.56
02SF3110	37 41.16	122 7.38	37.6	979955.66	-5.39	-6.68	0.3	1.13	-5.56	-6.21
02SF3130	37 41.16	122 7.32	39.3	979955.89	-5	-6.34	0.3	1.13	-5.22	-5.83
02SF3145	37 41.16	122 7.27	39.5	979956.17	-4.7	-6.05	0.3	1.13	-4.93	-5.51
02SF4007	37 41.30	122 7.40	36.1	979956.5	-4.9	-6.13	0	0.84	-5.3	-5.93
02SF4020	37 41.33	122 7.37	37.2	979956.7	-4.64	-5.91	0	0.85	-5.07	-5.68
02SF4040	37 41.36	122 7.32	34.8	979957.28	-4.33	-5.51	0	0.86	-4.66	-5.23
02SF4053	37 41.39	122 7.28	34.4	979957.56	-4.13	-5.3	0	0.87	-4.44	-4.98
02SF4B01	37 41.45	122 7.23	33.6	979958.1	-3.75	-4.9	0	0.89	-4.02	-4.51
02SF4B02	37 41.48	122 7.18	32.3	979958.53	-3.49	-4.59	0	0.9	-3.7	-4.15
02SF4B03	37 41.55	122 7.18	29.8	979958.9	-3.46	-4.47	0	0.92	-3.56	-4
02SF4B04	37 41.60	122 7.09	32.9	979959.25	-2.89	-4.01	0	0.94	-3.08	-3.45
02SF5001	37 41.63	122 7.06	34.6	979959.28	-2.74	-3.92	0	0.94	-2.99	-3.34
02SF5020	37 41.66	122 7.01	37.8	979959.33	-2.43	-3.72	0	0.95	-2.78	-3.09
02SF5040	37 41.70	122 6.96	37.6	979959.63	-2.21	-3.49	0	0.97	-2.54	-2.81
02SF5058	37 41.73	122 6.92	36.1	979959.98	-2.04	-3.28	0	0.98	-2.31	-2.54
02SF6001	37 41.77	122 6.86	35.8	979959.86	-2.25	-3.47	0	1	-2.49	-2.68
02SF6019	37 41.81	122 6.81	34.8	979960.37	-1.89	-3.08	0	1.02	-2.07	-2.21
02SF6040	37 41.85	122 6.77	35.5	979960.49	-1.77	-2.98	0	1.04	-1.95	-2.06
02SF6061	37 41.89	122 6.72	36.3	979960.49	-1.75	-2.99	0.01	1.07	-1.93	-1.99
02SF6080	37 41.93	122 6.67	37.4	979960.52	-1.67	-2.95	0.03	1.12	-1.84	-1.86
02SF6100	37 41.97	122 6.62	39.7	979960.5	-1.54	-2.89	0.07	1.18	-1.72	-1.7
02SF6119	37 42.00	122 6.58	62.8	979959.27	-0.64	-2.78	0.07	1.15	-1.66	-1.61
02SF6120	37 42.00	122 6.58	62.4	979959.19	-0.75	-2.88	0.07	1.15	-1.76	-1.71
02SF6GPS	37 42.02	122 6.54	77	979958.63	0.03	-2.6	0.11	1.17	-1.46	-1.38

Interpretation and Discussion

We interpret structures and stratigraphic relations along the SL seismic profiles on the basis of the combined reflection, refraction, well log, and gravity data. Many of these separate geophysical observations are consistent, leading to similar interpretations. Below, we discuss some of the more important issues related to earthquake hazards and ground-water-flow systems.

Structure of the San Leandro Basin and East Bay Plain

Consolidated basement rocks bound the aquifer system beneath the East Bay Plain. We interpret basement rocks to be the largely non-reflective rocks below depths of 200 to 1000 m along the seismic transect (Figs. 10 and 17; Fig 18). These rocks are probably Franciscan and older rocks that are not well stratified, and thus do not generate strong reflective energy. The poorly reflective probable Franciscan basement rocks are located below 800 to 1000 m depth southwest of meter 1300 of profile SL-1. At about meter 1300 of profile SL-1, basement rocks are vertically offset, east side up, several hundred meters along a zone of faults (Figs. 17 and 18). From about meter 1300 to about meter 2000, basement rocks rise along a series of faults to depths of about 400 m below land surface. The gravity anomaly along the southwestern 1300 m of profile SL-1 can be interpreted similarly, whereby basement abruptly rises by hundreds of meters over relatively short distances (Fig. 18). As observed within many strike-slip fault zones, there is greater vertical offset on some faults than other faults within a fault zone. From meter 2000 to about meter 3100, basement varies only slightly in depth (~50 m), but from about meter 3100 to about meter 4000, basement deepens by about 100 m. Although the

reflectors are not as well imaged along this segment of the transect as areas to the west, vertically offset reflectors suggest that basement deepens along one or more faults. Between meters 4000 and 4700 basement abruptly rises about 100-200 m to a depth of about 400 m. This also probably occurs along one or more faults. Between meter 5000 and to about meter 6000, basement rises to about 250 m depth, but because of large gaps in the seismic transect, we do not know if additional faults are present in this part of the transect. From about meter 6200 to the end of the seismic profile, basement abruptly rises to the near-surface along strands of the Hayward fault.

On the basis of the gravity and reflectivity patterns observed, we conclude that the deepest onshore part of the San Leandro Basin is about 800 to 900 m below the ground surface (bgs), and it extends northeastward about 1.4 km inland. Maximum depths of approximately 800 m for sub-horizontally layered sediments within the San Leandro Basin are consistent with observations by Marlow et al. (1999)**,** who also imaged sub-horizontal reflectors to depths of about 800 m near the center of the San Leandro Basin beneath the San Francisco Bay. However, on the basis of gravity modeling, Marlow et al. (1999) noted that relatively low-density (2.12 to 2.25 g/cm^3) rocks may extend to as much as 1.5 km depth. Although we cannot rule out the possibility that additional sediments underlie the sub-horizontal strata within the San Leandro Basin, the reflectivity pattern below 800-900 m near the bay is consistent with shallow-depth basement rocks imaged farther northeast along the transect. Furthermore, gravity modeling is consistent with shallow depths to basement on the northeast end of the profile and our imaged depth near the bay of 800-900 m.

Evidence for Faults Underlying the East Bay Plain

In several of the above sections of this report, we have highlighted evidence that infers the existence of faults beneath the East Bay Plain. In this section, we discuss the cumulative evidence. The principal evidence for the existence of buried faults beneath the East Bay Plain are the high-resolution reflection images, which show several zones along the transect where reflectors are vertically offset (Figs. 11, 19, 20, 21). We cannot exclude the possibility that some of the vertically offset reflections are artifacts related to non-linearity of the seismic profiles, but the combined velocity, gravity, and reflection data strongly suggest that the vertically offset reflectors are buried faults. Only selected individual faults are shown on figures 18 and 22. Further study likely may reveal additional faults. For purposes of discussion, we refer to the zones of vertically offset reflections as fault zones.

Fault zones are known to cause P-wave velocity anomalies, whereby lower seismic velocities occur within the fault zones relative to adjacent areas (Aki and Lee, 1976; Mooney and Luetgert, 1982; Catchings et al., 2002). Within the depth ranges of our seismic velocity measurements, we observe similar velocity anomalies within each of the probable near-surface East Bay Plain fault zones. Along profile SL-1, there are distinct low-velocity zones centered near meters 250 and 2250, and these low-velocity zones correlate with zones of near-surface, vertically offset reflections (Figs. 11 and 19). Similar, but less prominent low-velocity zones are observed along and between various profiles across the East Bay Plain.

The velocity data further suggest that several of the areas with vertically offset reflectors are zones of faulting by virtue of a relationship between the relative depth of fully saturated sediments and seismic velocity. As discussed above, unconsolidated, water-saturated sediments have minimum P-wave velocities of 1500 m/s (Nur, 1982; Schon, 1996), and lateral variations in the 1500 m/s velocity contours can be used to infer the relative depth of these sediments (Catchings et al.,1999; 2000a; Gandhok et al.,

1999). Along the East Bay Plain seismic transect, the depth to the 1500 m/s velocity contour (saturated sediments) increases within and southwest of the major near-surface fault zones (as inferred by vertically offset reflectors) (Fig. 19). Conversely, the saturated sediments are most shallow northeast of the near-surface fault zones. Ground-water flows from the northeast to the southwest across the East Bay Plain (San Francisco Bay Regional Water Quality Control Board, 2004). Thus, the inferred lateral variation in relative depth to the ground-water table, whereby it is shallower to the northeast and deepens to the southwest of fault zones, is expected if the offset reflectors are ground-water barriers caused by faulting (Fig. 19). Mechanical disruption of sediments in fault zones reduces seismic velocity in a manner consistent with the seismic velocity profiles. Available ground-water-level data are areal1y too sparse and temporally too widely spread to definitively confirm or refute interpretations of water table depth derived from the seismic velocity data.

Gravity modeling is consistent with the seismic reflection image, whereby the gravity model infers near-vertical offsets in stratigraphic layers, especially near the northern end of the San Leandro Basin. These near-vertical offsets in stratigraphy suggest a number of fault strands underlie the East Bay Plain between the San Francisco Bay and the Hayward fault. Additional seismic profiling and paleoseismic trenching are needed to confirm the imaged fault zones, but the cumulative reflection, velocity, and gravity data presented in this study strongly suggest multiple fault strands underlie the East Bay Plain.

Length of Faults

Although the cumulative data suggest multiple fault strands underlie the East Bay Plain, the lengths of these faults are unknown. Fault length is important for earthquake hazard assessment because fault length is directly related to the maximum magnitude earthquake the faults can generate. Sparsely spaced earthquake hypocenters recorded between 1984 and 2004 (ANSS, 2004; Zoback and Olson, 1995; Simpson et al., 2004) are consistent with sub-alluvial faults that may extend from the southern Santa Clara Valley to the northern part of the San Francisco Bay. On the basis of vertically offset reflectors observed along the East Bay Plain seismic transect, we suggest that the fault zone bounding the San Leandro Basin on the northeast at about meter 1300 of the SL-1 profile may be the most laterally extensive of the East Bay Plain faults, with the exception of the Hayward fault. The lack of significant southwestward dipping strata within and near the northeastern end of the San Leandro Basin suggests that the northeastern end of the basin formed along a zone of faults with a significant (~500 m) component of vertical movement rather than a uniformly down-warping central basin as suggested by Marlow et al. (1999). Such a large vertical offset suggests that the fault may be laterally extensive, and a growing body of geophysical evidence (Catchings et al., in prep.) suggests that the bounding fault may be an extension of the Silver Creek Fault zone. The Silver Creek fault zone has been mapped and imaged farther south within the Santa Clara Valley (Bortugno et al., 1991; Catchings et al., 2000b; R. Williams, Pers. Comm, 2005), and older ground-water and gravity data suggest that the fault extends as far north as Union City (CDWR, 1967). For purposes of discussion in the report, we refer to the fault bounding the San Leandro Basin as the East Bay fault zone, which would be more than 60 km long if it is contiguous with the Silver Creek fault zone.

Recency and Extent of Faulting Across the East Bay Plain

If active, the East Bay fault zone may be capable of generating earthquakes with magnitudes comparable to or larger than those of the Hayward fault, based on comparison of the lengths of the faults. The shallow depths to which the East Bay fault zone offsets strata along profile SL-1 suggests that the fault has been active relatively recently (Figs. 11, 20, and 21). Furthermore, low-level seismicity in the vicinity of the imaged faults (Zoback and Olson, 1995; Simpson et al., 2004) indicates that the faults are probably active (Fig. 22). At shallow depths (upper 400 m), vertically offset strata along the seismic transect indicate that other faults underlie the East Bay Plain between the East Bay and Hayward faults; we refer to these faults as middle faults. Although the middle faults may be separate faults, they may also be strands that merge with either the East Bay or Hayward fault zones at depth. Earthquake hypocenters indicate that some of the faults are deep seated (Simpson et al., 2004) and are unrelated to the Hayward fault above Moho depths.

Aquifers

Izbicki et al. (2003) list four principal zones in the East Bay Plain ground-water basin that may be time correlative with aquifer sediments in the Niles Cone ground-water basin, the Newark (9-40 m bgs), Centerville (36 to 67m bgs), Fremont (73 to 122 m bgs), and the Deep aquifers (152 to 198 m bgs). From comparisons among the seismic images and borehole electric and lithologic logs acquired near the seismic transect, the Deep aquifer correlates well with specific reflectors, but the Newark, Fremont, and Centerville aquifers do not stand out prominently on some electric logs, making their exact depth range poorly determined (Fig. 13). As such, there is some ambiguity in correlating the reflection horizons on the seismic image with specific layers of the Newark, Centerville, and Fremont aquifers. Many investigators have been unable to trace individual permeable beds of the Newark, Centerville, and Fremont aquifers between boreholes and wells in the East Bay Plain (Izbicki et al., 2003). In this report, we do not specifically identify the Newark, Centerville and Fremont aquifers; rather, we identify a series of reflectors that encompasses the depth ranges believed to include discontinuous permeable lenses of sediment that are time-correlative with the Newark, and the Centerville/Fremont aquifers as defined in the Niles Cone ground-water basin to the south. Partly consolidated sedimentary deposits having low porosity and low permeability are believed to underlie the major aquifers in the study area (Marlow et al., 1999**),** but we have not attempted to identify individual stratigraphic layers or permeable beds within the sediments underlying the Deep aquifer.

Near-coincident logged wells and the seismic transect show that aquifer zones often correlate with specific groups of reflectors. Some of these reflectors can be traced across the entire seismic transect, suggesting that the stratigraphic horizons that often contain permeable deposits are continuous across the East Bay Plain. The correlation between well logs and the reflection profile is best for the Deep aquifer, the thickest and most persistent permeable horizon of permeable sediments in the East Bay Plain (Figs. 13 and 21). A group of reflectors that correlate with the Deep aquifer varies in thickness across the East Bay Plain but is thickest near the SF Bay. Short-normal resistivity logs show that some layers of the Deep aquifer are consistently resistive, suggesting that they consist of clean, fresh-water–bearing sand and gravel layers. To the northeast, near San Leandro High School, there may be fewer coarse-grained layers within the Deep aquifer sediments.

The hydraulic properties and quality of water within sediments that are strong reflectors beneath the Deep aquifer, seen most prominently southwest from meter 1300 of profile SL-1 and along profile SL-6, have not been determined. Historical well records indicate that several wells southwest from meter 1300 of profile SL-1 were drilled deeper than the bottom Deep aquifer in the early 1900s but well records do not identify perforated intervals of casing or water production rates for these deep wells. A down-well television scan (Michael Burke, Fugro West, written communication, 1997) of well 3S3W-14K2, drilled 993 feet deep in 1919, indicated that the steel well casing was perforated at depths below the Deep aquifer but other historical information is unavailable. Because well 14K2 is filled with sediment to 813 feet below land surface and much of the steel casing is encrusted with scale, the identification of perforated intervals by TV scan or hydraulic testing to determine hydraulic characteristics of sediments underlying the Deep aquifer are infeasible. If the reflectors beneath the Deep aquifer are Pliocene sediments (as Marlow and others (1999) suggest underlie Pleistocene deposits in the San Leandro basin) or if the reflectors are partly consolidated rocks (as encountered by deep wells near Bay Farm Island, north from the study area (Izbicki and others, 2003)), it is unlikely that the reflectors are aquifer zones that might be developed for water supply or artificial storage of water.

East Bay Plain Faults, Ground-Water Flow, and Infrastructure

In this report, we note several important features of the subsurface structure and stratigraphy that may impact ground-water flow and infrastructure across the East Bay Plain.

Hydraulic head data (Izbicki et al., 2003) indicate that ground water generally flows through shallow sediments from the hills on the east to the bay on the west. If the faults imaged on the reflection profile trend parallel to the Hayward fault, as expected, they may retard the flow of ground water toward the bay to some extent. Available ground-water-level data are areally too sparse to definitively confirm or refute interpretations of water table depth derived from the seismic velocity data.

Sedimentary units containing the Newark, Centerville/Fremont, and Deep aquifers are probably all affected by the fault zones, as their thickness and depth below ground surface appear to vary across the fault zones. If the faults hydraulically restrict westerly ground-water flow, they may partly compartmentalize the aquifer system, causing the performance of ground-water facilities to vary from operations as designed. A better understanding of the 3-dimensional aquifer structure and hydraulic continuity is needed to assess the effect of faults within the East Bay Plain.

Movement on faults underlying the East Bay Plain may restrict lateral ground-water flow. During future earthquakes, vertical movements of just a few meters may offset aquifers enough to affect flow across the fault zones. Similarly, such movements may hamper water-utility infrastructure such as pipelines. A more complete understanding of the locations and orientations of active faults within the East Bay Plain may allow for improvements before future damaging earthquakes. Such planning was implemented along the Alaska oil pipeline where it crossed four major fault zones identified from scientific investigations conducted in the 1970's. During the November 3, 2002 M. 7.9 Denali earthquake (Eberhart-Phillips et al., 2003), nearly 4 m of horizontal and 0.75 m of vertical offset occurred across the fault, but because of special engineering along the fault zones, there was no disruptive damage to the pipeline (Cluff and Slemmons, 2002). Similar engineering could be implemented across the East Bay Plain faults if their locations throughout the East Bay were determined.

Suggestions for Future Work

Movement on fault zones beneath the East Bay Plain could affect ground-water-flow directions. A concerted effort to locate active faults beneath the East Bay Plain should be undertaken so that production wells can be strategically placed to minimize disruptions from future earthquakes on the subsurface faults. A combination of strategically placed water-level observation wells, high-resolution seismic imaging, INSAR imaging, and paleoseismological trenching may be a useful approach.

Acknowledgements:

We thank the East Bay Municipal Utility District (EBMUD) for providing partial funding for this investigation and assisting with access. We also thank Alameda County, the City of San Leandro, San Leandro High School, and EBMUD for permits and access. We thank Coyn Criley, Coye Criley, Dave Cornwell, Shane Detweiler, Joel Fassbinder, Sam Gudino, Wendy Hauso, Amy Padovani, A.S.S.S.R.S. Prashad, Friedericke Schmitz, Camgna Thach, and V Shridher for field assistance. Thanks to Jim Lienkamper and Jack Boatwright, who provided critical reviews. We thank Bob Bainer of Lawrence Livermore National Laboratory for providing seismic sources along 163rd Avenue in San Leandro, and we thank IRIS-PASSCAL for providing one of the multichannel seismographs used to record the data. We thank Kelly McPherson and Tim Dawson, USGS, for surveying the locations of shot points and sensor arrays.

References

2003 U.S. Census; http://quickfacts.census.gov/qfd/states/06/06085.html

Aki, K., and W. H. K. Lee, 1976, Determination of three-dimensional velocity anomalies under a seismic array using P-arrival times from location earthquakes, I. A homogeneous initial model, J. Geophys. Res., 81, 4381-4399.

Advanced National Seismic System (ANSS) Catalog, 2004, anss@quake.geo.berkeley.edu

Atwater, B. G., Ross, B. E., Wehmiller, J.F., 1981, Stratigraphy of the late Quaternary estuarine deposits and amino acid stereochemistry of oyster shells beneath San Francisco Bay, California: Quaternary Research, v. 16, p. 181-200**.**

Aydin, A., 1982, The East Bay hills, a compressional domain resulting from interaction between the Calaveras and Hayward-Rogers Creek faults in E. W. Hart et al. (Eds), Proceedings, Conference on Earthquake Hazards in the Eastern San Francisco Bay Area: California Division of Mines and Geology Special Publication 62, p.11-21.

Bortugno, E.J., McJunkin, R.D., and Wagner, D.L., 1991, Map showing recency of faulting, San Francisco-San Jose quadrangle, 1:250,000: Department of Conservation, Division of Mines and Geology Regional Geologic Map Series, Map 5A, Sheet 5.

Brouwer, J., and Helbig, K., 1998, Shallow high-resolution reflection seismics. In: Helbig, K., Treitel, S. (Eds.), Handbook of Geophysical Exploration: Seismic Exploration, Vol. 19, Elsevier, New York, New York, 391 p.

California Department of Water Resources (CDWR), 1967, Evaluation of Ground Water Resources, South Bay, Appendix A: Geology: Bulletin 118-1, 153 p.

California Department of Water Resources (CDWR), 1975, Evaluation of groundwater resources, south San Francisco Bay, Volume III, northern Santa Clara County area: Bulletin No. 118-1, various pagination

California Department of Water Resources, Bulletin, 118-180, 1980, Ground water basins in California, 73 p.
Catchings, R.D., G. Gandhok, M. R. Goldman, E. Horta, M. J. Rymer, P. Martin, and A. Christensen, 1999, Subsurface, high-resolution seismic images from Cherry Valley, San Bernardino County, California: implications for water resources and earthquake hazards, U.S. Geol. Surv. Open-File Rept. 99-26, 57 pp.
Catchings, R.D., B.F. Cox, M. R. Goldman, G. Gandhok, M. J. Rymer, J. Dingler, P. Martin, A. Christensen, and E. Horta, 2000a, Subsurface structure and seismic velocities as determined from high-resolution seismic imaging in the Victorville, California area: implications for water resources and earthquake hazards, U.S. Geol. Surv. Open-File Rept., 00-123, 70 pp.
Catchings, R.D., M. R. Goldman, G. Gandhok, M. J. Rymer, and D. H. Underwood, 2000b, Seismic imaging evidence for faulting across the northwestern projection of the Silver Creek fault, San Jose, California, U. S. Geol. Surv. Open-File Rept., 00-125, 29 p.
Catchings, R. D., M. J. Rymer, M. R. Goldman, J. A. Hole, R. Huggins, and C. Lippus, 2002, High-resolution seismic velocities and shallow structure of the San Andreas fault zone at Middle Mountain, Parkfield, California, Bull. Seis. Soc. Am, 92, 2493-2503
Carmichael, R. S., 1989, Practical Handbook of Physical Properties of Rocks and Minerals, CRC Press, Boca Raton, Ann Arbor, Boston.
Ch2M-Hill, Inc., 2000, Regional hydrogeologic investigation of the south East Bay Plain, Oakland, California.
Cluff, L. S., and D. B. Slemmons, 2002, Trans Alaska pipeline design accommodations November 3, 2002 Magnitude 7.9 earthquake, EOS Trans. AGU, 83, S72F-1329
Dobrin, M. B., and C. H. Savit, 1988, Introduction to geophysical prospecting, McGraw-Hill Book Co., San Francisco, California, 867 pp.
Figuers, S., 1998, Groundwater study and water supply history of the East Bay Plain, Alameda and Contra Costa counties, California: Livermore, California, Norfleet Consultants, 90 p.
Eberhart-Phillips, D. and 28 others, 2003, The 2002 Denali Fault earthquake, Alaska: A large magnitude, slip-partitioned event, Science, 300, 111301118.
Gandhok, G., R. D. Catchings, M. R. Goldman, E. Horta, M. J. Rymer, P. Martin, and A. Christensen, 1999, High-Resolution Seismic Reflection/Refraction Imaging from Interstate 10 to Cherry Valley Boulevard, Cherry Valley, Riverside County, California: Implications for Water Resources and Earthquake Hazards, U.S. Geological Survey Open-File Report 99-320, 52 pp., http://geopubs.wr.usgs.gov/open-file/of99-320/
Graymer, R.W., 2000, Geologic map and map data base f the Oakland metropolitan area, Alameda, Contra Costa, and San Francisco counties, California: U. S. Geological Survey, Misc. Field. Studies Map MF-2342, 1 sheet, scale 1:50,0000, http://geopubs.wr.usgs.gov/map-mf/mf2342/
Hole, J. A., 1992, Nonlinear high-resolution three-dimensional seismic traveltime tomography, Journal of Geophysical Research, v. 97, p. 6553-6562.
Howard, A. D., 1979, Geologic history of middle California: California Natural History Guides: 43, 113 p.
Izbicki, J.A, Borchers, J.W., Leighton, D.A., Kulongoski, J., Fields, L., Galloway, D.L., and Michel, R.L., 2003, Hydrogeology and geochemistry of aquifers underlying the San Lorenzo and San Leandro areas of the East Bay Plain, Alameda County, California, U.S. Geol. Surv. Water Resources Investigations Report 02-4259, http://pubs.usgs.gov/wri/wrir024259/text.html
Koltermann, C. E., and Gorelick, S. M., 1992, Paleoclimatic signature in terrestrial flood plain deposits: Science, v. 256, p. 1775-1782.

Luhdorff and Scalmanini Consulting Engineers, 2003, East Bay Plain aquifer test project: South East Bay Plain and Niles Cone ground-water basins, 39 p.

Maslonkowski, Dennis (1988). Hydrogeology of the San Leandro and San Lorenzo Alluvial Cones of the Bay Plain Groundwater Basin, Alameda County, California, Masters of Science Thesis, San Jose State University, 143 p.

Marlow, M.S., R.C. Jachens, P.E. Hart, P.R. Carlson, R.J. Anima, J.R. Childs, 1999, Development of the San Leandro synform and neotectonics of the San Francisco Bay block, California, Marine and Petroleum Geology, v. 16, p. 431-442.

Mooney, W.D., and J. H. Luetgert, 1982, A seismic refraction study of the Santa Clara Valley and southern Santa Cruz Mountains, west-central California, Bull. Seism. Soc. Am., 72, 901-909

Mooney, W.D., and A. Ginzburg, 1986, Seismic measurements of the internal properties of fault zones, Pure and Applied Geophysics, 124, p. 141-157

Muir, K. S., 1993, Classification of groundwater recharge potential in the East Bay Plain area, Alameda County, California: Alameda County Flood Control and Water Conservation District, Hayward, Calif., C-92-320, 10 p.

Nur, A. (1982). Notes on wave propagation in porous rocks, Stanford Rock Physics Progress Report, January 1982, v. 13, 121 pp. Stanford University, Stanford, CA,

Ponce, D.A., 2001, Principal facts for gravity data along the Hayward fault and vicinity, San Francisco Bay area, northern California, U.S. Geological Survey Open-File Report 01-124, 29 pp., http://geopubs.wr.usgs.gov/open-file/of01-124/

Ponce, D.A., T. G. Hilderbrand, and R. C. Jachens, 2003, Gravity and magnetic expression of the San Leandro Gabbro with implications for the geometry and evolution of the Hayward Fault zone, Northern California, Bull. Seism. Soc. Am., 93, 14-26

Ross, B. E., 1977, The Pleistocene history of the San Francisco Bay along the southern crossing: Master of Science thesis, San Jose State University, 121 p.

Rogers, J. D., and Figuers, S.H., 1991, Engineering geologic site characterization of the greater Oakland-Alameda area, Alameda and San Francisco counties, California: Pleasant Hill, Calif., Rogers/Pacific, Inc., 59 p.

San Francisco Bay Regional Water Quality Control Board, 2004, East bay plain ground water basin beneficial use evaluation report, Final report.

Schon, J. H., 1996, Physical Properties of Rocks: Fundamentals and Principals of Petrophysics, Handbook of Geophysical Exploration, Seismic Exploration v. 18, Elsevier Science, Inc., Tarrytown, N. Y.

Simpson, R.W., R. W. Graymer, R.C. Jachens, D.A. Ponce, C.M. Wentworth, 2004, Cross-sections and maps showing double-difference relocated earthquakes from 1984-2000 along the Hayward and Calaveras faults, California, U.S. Open-File Report 2004-1083a (http://pubs.usgs.gov/of/2004/1083/explanation.html#datasourceseqs).

Sloan, D., 1992, The Yerba Buena mud: Record of the last-interglacial predecessor of San Francisco Bay, California: Geological Society of America, v.104, p. 716-727.

Stanley, R.G., Jachens, R.C., Lillis, P.G., McLaughlin, R.J., Kvenvolden, K.A., Hostettler, F.D., McDougall, K.A., and Magoon, L.B., 2002, Subsurface and Petroleum Geology of the Southwestern Santa Clara Valley ("Silicon Valley"), California: U.S. Geological Survey Professional Paper 1663, 55 p., http://geopubs.wr.usgs.gov/prof-paper/pp1663/

Trask, P. D., and Rolston, J. W., 1951, Engineering geology of San Francisco Bay, California: Bulletin of the Geological Society of America, v. 82, p. 1079-1110.

Unruh, J. R. and Lettis, W. R.,1998, Kinematics of transpressional deformation in the eastern San Francisco Bay region, California. Geology, v. 26, p.19-22.

Waldhauser, F., and W. L. Ellsworth, 2000, A double-difference earthquake location algorithm: Method and application to the northern Hayward Fault, California, Bull. Seism. Soc. Am., 90, 1353-1368.

Waldhauser, F., and W. L. Ellsworth, 2002, Fault structure and mechanics of the Hayward Fault, California from double-difference earthquake locations, J. Geophys. Res., 107, 3-15.

Wallace, R. E., 1990, General features in the San Andreas fault system, California, in The San Andreas Fault System, California, R. E. Wallace, ed., U.S. Geol. Surv. Prof. Paper 1515, p. 3-12., http://education.usgs.gov/california/pp1515/

Zoback, M. L., Olson, J. A., and Jachens, R. C., 1995, Seismicity and basement structure beneath south San Francisco Bay, California in Sangines, E. M., Andersen, D. W., and Buising, A. V., eds., Recent geologic studies in the San Francisco Bay area: Pacific section of the Society of Economic Paleontologists and Mineralogists, Book 76, 278 p.

Figures

Figure 1. Map of the San Francisco Bay area, with major fault zones and cities of the East Bay Plain and Niles Cone areas. The location of figure 2 and the general location of the seismic transect discussed in the report are shown by the red box. Various cities within the East Bay Plain are listed: A=Alameda, F=Fremont, H=Hayward, N=Newark, O= Oakland, SL= San Lorenzo, SLe=San Leandro, UC=Union City. Major roads are shown in gray, and major fault zones are shown in yellow.

Figure 2. Parts of the USGS 7.5-minute San Leandro and Hayward topographic maps showing the locations of the East Bay Plain (SL) seismic transect. Individual segments of the transect are labeled SL-1 through SL-6. The dashed line shows the general placement of the seismic arrays.

Figure 3. (a) Geophone elevation along seismic profile SL-1. Elevation is relative to the topographically lowest geophone along the profile. (b) Variation of geophones from a line that connects the first and last geophone along the profile. (c) Shot point elevation along seismic profile SL-1. Elevation is relative to the topographically lowest shot point along the profile. (d) Variation of shot points from a line connecting the first and last shot point along the profile. (e) Fold as a function of distance along the SL-1 seismic profile.

Figure 4. (a) Geophone elevation along seismic profile SL-2. Elevation is relative to the topographically lowest shot point along the profile. (b) Variation of geophones from a line that connects the first and last geophone along the profile. **(c)** Shot point elevation along seismic profile SL-2. Elevation is relative to the topographically lowest shot point along the profile. (d) Variation of geophones from a line connecting the first and last shot point along the profile. **(e**) Fold as a function of distance along the SL-2 seismic profile.

Figure 5. (a) Geophone elevation along seismic profile SL-3. Elevation is relative to the topographically lowest shot point along the profile. (b) Variation of geophones from a line that connects the first and last geophone along the profile. (c) Shot point elevation along seismic profile SL-3. Elevation is relative to the topographically lowest shot point along the profile. (d)Variation of geophones from a line connecting the first and last shot point along the profile. (e) Fold as a function of distance along the SL-3 seismic profile.

Figure 6. **(**a**)** Geophone elevation along seismic profile SL-4. Elevation is relative to the topographically lowest shot point along the profile. (b) Variation of geophones from a line that connects the first and last geophone along the profile. (c) Shot point elevation along seismic profile SL-4. Elevation is relative to the topographically lowest shot point along the profile**.** (d) Variation of geophones from a line connecting the first and last shot point along the profile. (e) Fold as a function of distance along the SL-4 seismic profile.

Figure 7. (a) Geophone elevation along seismic profile SL-5. Elevation is relative to the topographically lowest shot point along the profile. (b) Variation of geophones from a line that connects the first and last geophone along the profile. (c) Shot point elevation along seismic profile SL-5. Elevation is relative to the topographically lowest shot point along the profile. (d) Variation of geophones from a line connecting the first and last shot point along the profile. (e) Fold as a function of distance along the SL-5 seismic profile.

Figure 8. (a) Geophone elevation along seismic profile SL-6. Elevation is relative to the topographically lowest shot point along the profile. (b) Variation of geophones from a line that connects the first and last geophone along the profile. (c) Shot point elevation along seismic profile SL-6. Elevation is relative to the topographically lowest shot point along the profile. (d) Variation of geophones from a line connecting the first and last shot point along the profile. (e) Fold as a function of distance along the SL-6 seismic profile.

Figure 9. P-wave seismic velocity model along the East Bay Plain seismic (SL) transect with various landmarks shown. Cumulative distance is shown along the bottom. Note that in profile view, profiles SL-3 and SL-4 overlap (see fig. 2), but lateral distance between the beginning and end of SL-3 and SL-4, respectively, is several hundred meters. Distance along individual profiles (see figure 2) are shown above the figure. Velocities are in m/s, and depth and distance are in meters. Depth is relative to the topographically lowest geophone along each seismic profile. The 1500 m/s contour, which probably shows lateral variations in the relative depth to continuously saturated sediments (water depths), is shown in white. Because of smoothing in the velocity model, absolute depths of the water table may not be accurate.

Figure 10. A relatively low-frequency (30-60-200-400 Hz) composite seismic reflection image of the upper 1500 m along the East Bay Plain seismic transect. Stacking fold, elevation, and various landmarks are shown above the figure. Each seismic profile, SL-1 through SL-6, is shown relative to its distance from the southeastern-most geophone along the profile. However, distance between profiles SL-3 and SL4 includes lateral distance between the ends of the profiles. Depth and distance are in meters. Depth is relative to the lowest point along each seismic profile.

Figure 11. A relatively high-frequency (50-100-200-400 Hz) composite seismic reflection image along the East Bay Plain, plotted as in figure 10. Only the upper 500 m are shown along the profile because the higher frequencies generally limit the depth of reflection imaging. The locations of various wells with available geophysical and lithologic logs and various landmarks are shown above the figure.

Figure 12. Photograph of the area encompassing the East Bay Plain seismic transect and selected nearby wells. Seismic profiles are shown in red, and perpendicular projections of the wells to the seismic profile are shown in yellow. The base map is modified from the USGS San Leandro and Hayward, California 7.5-minute orthophoto maps.

Figure 13. Seismic image from figure 11 with short-normal resistivity logs (red) and simplified lithologic logs (multi-colored) projected onto the seismic image at perpendicular distances. Sedimentary layers that contain aquifers in some places are shown in blue. Lateral extensions of the aquifer-bearing layers are inferred based on laterally continuous or nearly continuous reflectors. Continuity of reflectors between the profiles is only inferred.

Figure 14. Topographic map of the central East Bay Plain, showing the general location of the East Bay Plain (SL) seismic transect, along which our gravity model is constructed (orange), and the profile along which the model (profile C-C"; in black) of Ponce et al., (2003) is constructed. The yellow dots show earthquake epicenters with size proportional to magnitude. The red line shows the approximate surface trace of the Hayward fault (from Ponce et al., 2003).

Figure 15. (a) Observed (blue) and calculated (red) Bouguer gravity anomaly along the East Bay Plain seismic transect. (b) Gravity model based on seismic-reflection-determined depths to basement rocks (green) and the best fit to the Bouguer gravity data. Density (in parentheses) is in grams per cubic centimeter. Because distance between profiles SL-3 and SL-4 is mostly lateral distance, basement depths are extrapolated in that area.

Figure 16. Observed (black) and calculated (red) (a) magnetic and (b) gravity anomaly along profile C-C' (see figure 14). (c) Gravity and magnetic models along profile C-C' (from Ponce et al., 2003). Geologic symbols: Qa, Quaternary alluvium and related low-density materials; Tn, Neroly Sandstone; Ts, undifferentiated Tertiary sedimentary rocks; KJF, Franciscan Complex; Kjm, Joaquin Miller Fm; Kjk, Knoxville Fm; Ko, Oakland conglomerate; Ks, undifferentiated Cretaceous sedimentary rocks; Jb, basalt; Jgb, gabbro; Jpb, pillow basalt; jsv, quartz keratophyre; sp, serpentinite; sp-px, pyroxenite. Geographic and other symbols: SF Bay, San Francisco bay; SL Res., San Leandro reservoir, Inverted red triangles, recent trace of Hayward Fault (HF) and Chabot Fault (CF); D, density in grams/cubic centimeter; S, susceptibility in CGS units; Drill-hole symbol, thickness of offshore sedimentary basin from seismic and gravity data (Marlow et al., 1999); +, seismicity from relocated hypocenters using double-difference relocation method within 5 km of the profile (Waldhauser and Ellsworth, 2000; 2002). The red rectangle shows the approximate location of the East Bay Plain seismic transect (2 km depth).

Figure 17. (a) Composite seismic image (30-60-200-400 Hz) from figure 10 with interpreted layer sequences (blue) containing ground-water aquifers, electric and lithologic well logs, faults (red), and basement topography, as modeled with our SL gravity model (yellow) and the model of Ponce et al. (2003**)** (orange) north of the SL seismic profile. The basement topography modeled by Ponce et al. (2003**)** is extrapolated (dashed line) along segments of the SL profile that do not trend northwestward.

Figure 17 (b) Seismic reflection image along profile SL-1, plotted with lower frequencies (25-50-400-800 Hz) than in figure 17a. Gravity-inferred basement topography (orange – Ponce et al., 2003; yellow = SL gravity model) is superimposed on the reflection image.

Figure 18. Interpretative cross section (including wells, electric logs, sedimentary sequences containing aquifers, faults, etc), with basement as inferred from the SL gravity model (black-green). Basement as inferred from the model of Ponce et al. (2003**)** north of the SL profile is shown in orange. The basement topography modeled by Ponce et al. (2003) is extrapolated (dashed line) along segments of the SL profile that does not trend northwestward. Areas along the East Bay transect with apparent shallow-depth faults are outlined in red above the interpretative cross section.

Figure 19. (a) Velocity model (from figure 9) along the East Bay Plain seismic transect, with the 1500 m/s velocity contour (lateral variation in the relative depth of continuously saturated sediments) shown in white (b) Relatively high-frequency (50-100-200-400 Hz) seismic reflection image (from figure 11) with borehole electric logs and interpretative sedimentary sequences that contain aquifers in places. Note that low-velocity zones correlate with apparent zones of near-surface (upper 80 m) faulting.

Figure 20. A relatively low-frequency (25-50-400-800 Hz) migrated seismic reflection image along profile SL-1. Note the numerous vertically offset layers, particularly those between meters 200 and 400 and meters 1600 and 2500. The red arrows are located over two zones of faulting that are most apparent at about 400 m depth.

Figure 21. A relatively intermediate-frequency (35-70-200-400 Hz) migrated seismic reflection image of all profiles along the East Bay Plain seismic transect. Borehole resistivity and lithologic well logs and interpreted sedimentary sequences that sometimes contain aquifers are shown on the seismic section. The pink line in the upper 50 m shows the 1500 m/s velocity contour along the seismic transect (interpolated between seismic profiles) as determined from the SL velocity model (fig. 9).

Figure 22. Seismic reflection image (from figure 17b) along profile SL-1 with hypocenters of earthquakes within 3 km of the profile. Earthquake locations are from the Northern California Catalog (ANSS, 2004). Note that the hypocenters from nearby small earthquakes largely align with the northeastern edge of the San Leandro Basin. Earthquakes beyond 3 km from the SL profile are shown in figure 14.

Appendixes

Appendix A.

Coordinates of the beginning and end of each profile in latitude and longitude and in UTM coordinates.

LINE	LAT	LONG	Easting	Northing
Start SL1	37:40.1174	-122:09.8860	573661	4169377
End SL1	37:41.0649	-122:08.3701	575873	4171150
Start SL2	37:41.0984	-122:08.3085	575963	4171212
End SL2	37:41.0719	-122:07.8083	576698	4171170
Start SL3	37:41.0727	-122:07.7788	576742	4171172
End SL3	37:41.1566	-122:07.3337	577394	4171333
Start SL4	37:41.2864	-122:07.4765	577182	4171571
End SL4	37:41.3865	-122:07.3429	577377	4171758
Start SL5	37:41.6257	-122:07.1288	577687	4172203
End SL5	37:41.7245	-122:06.9805	577903	4172388
Start SL6	37:41.7864	-122:06.9004	578020	4172504
End SL6	37:42.0097	-122:06.6289	578415	4172920

Appendix B

Distances and elevations along East Bay Seismic Profile 1 (SL-1).
Measurements are relative to the first receiver point at the west end of Profile SL-1.

Station No.	Receiver Dist. (m)	Receiver Elev. (m)		Station No.	Shot Dist. (m)	Shot Elev. (m)
1	0	0				
2	3.4	0.04				
3	7.36	0.06				
4	10.81	0.13				
5	14.71	0.13				
6	19.56	0.17				
7	24.46	0.17				
8	29.21	0.31				
9	34.16	0.53		9	34.06	0.46
10	39.01	0.59		10	38.76	0.59
11	43.96	0.57		11	43.81	0.59
12	48.87	0.63		12	48.66	0.62
13	53.77	0.74		13	53.47	0.74
14	58.62	0.74		14	58.37	0.73
15	63.52	0.67		15	63.22	0.68
16	68.37	0.74		16	68.17	0.77
17	73.52	0.78		17	73.22	0.82
18	78.27	0.81		18	78.02	0.82
19	83.02	0.82		19	82.92	0.84
20	88.07	0.81		20	87.87	0.87
21	92.87	0.86		21	92.62	0.9
22	97.72	0.87		22	97.47	0.91
23	102.67	0.9		23	102.42	0.9
24	107.67	0.89		24	107.38	0.88
25	112.53	0.9		25	112.22	0.86
26	117.37	0.89		26	117.08	0.86
27	122.28	0.9		27	121.87	0.9
28	127.18	0.96		28	126.92	0.99
29	132.12	0.97		29	131.83	0.96
30	136.88	1.01		30	136.78	1.02
31	141.78	1.02		31	141.58	1
32	146.63	0.99		32	146.53	1.01

33	151.58	0.95		33	151.33	0.97
34	156.43	0.95		34	156.28	0.97
35	161.33	0.97		35	161.03	1
36	166.18	0.9		36	165.93	0.95
37	171.03	0.95		37	170.93	0.95
38	175.98	0.95		38	175.68	1
39	180.88	0.96		39	180.58	0.97
40	185.69	0.98		40	185.54	1.05
41	190.58	1.03		41	190.39	1.08
42	195.43	1.01		42	195.18	1.05
43	200.33	1.02		43	200.29	1.03
44	205.18	1.05				
45	210.09	1.09		45	209.93	1.06
46	215.08	1.09		46	214.99	1.04
47	220.04	1.16		47	220.04	1.13
48	224.99	1.2		48	224.94	1.18
49	229.94	1.28		49	230.04	1.25
50	234.99	1.25		50	235.14	1.29
51	239.99	1.13		51	239.94	1.19
52	244.94	1.06		52	244.84	1.17
53	249.99	1.12		53	249.93	1.18
54	254.94	1.09		54	254.84	1.21
55	259.99	1.09		55	260.14	1.17
56	264.89	1.11		56	264.89	1.11
57	269.98	1.22		57	269.79	1.17
58	274.83	1.24		58	274.94	1.18
59	279.98	1.18		59	279.83	1.15
60	284.89	1.13		60	285.03	1.07
61	289.99	1.21		61	289.88	1.19
62	294.88	1.2		62	294.79	1.22
63	299.99	1.16		63	299.64	1.26
64	305.14	1.26		64	304.84	1.33
65	309.89	1.18		65	309.84	1.16
66	314.84	1.29		66	314.89	1.29
67	319.89	1.23		67	319.98	1.31
68	324.93	1.25		68	324.89	1.29
69	329.94	1.37		69	330.13	1.36
70	334.48	1.34				
71	339.84	1.31		71	339.83	1.41
72	344.84	1.29		72	344.89	1.29
73	349.84	1.32				
74	354.84	1.27		74	354.79	1.3
75	359.84	1.37		75	359.79	1.35
76	364.78	1.34		76	364.98	1.31
77	369.78	1.32				
78	374.78	1.35		78	374.89	1.3
79	379.84	1.3		79	379.89	1.35
80	384.84	1.3		80	384.83	1.36
81	389.94	1.4		81	389.68	1.33
82	394.89	1.4		82	394.89	1.29
83	399.89	1.36		83	400.08	1.32
84	404.84	1.43		84	404.99	1.31
85	409.84	1.43		85	409.83	1.4
86	414.78	1.46		86	414.83	1.4
87	419.89	1.41				
88	424.84	1.56		88	424.89	1.53
89	429.78	1.51		89	429.89	1.51
90	434.89	1.51		90	434.89	1.45
91	440.03	1.48				
92	444.74	1.37		92	444.89	1.36
93	449.93	1.35		93	449.83	1.34
94	454.93	1.4				
95	459.64	1.33		95	459.64	1.35
96	464.59	1.32		96	464.84	1.38
97	469.84	1.35		97	469.73	1.35
98	474.84	1.29		98	474.73	1.44
99	479.74	1.35		99	479.84	1.44
100	484.89	1.32		100	484.64	1.37
101	489.89	1.41		101	489.58	1.49
102	494.89	1.44		102	494.73	1.47

103	499.83	1.35		103	499.94	1.37
104	504.79	1.43				
105	509.79	1.38		105	509.84	1.41
106	514.68	1.34		106	514.64	1.32
107	519.83	1.35		107	519.73	1.36
108	524.78	1.39		108	524.83	1.38
109	529.78	1.4				
110	534.74	1.43		110	534.74	1.38
111	539.84	1.35		111	539.69	1.36
112	544.84	1.38		112	544.69	1.35
113	549.79	1.45		113	549.69	1.39
114	554.73	1.48		114	554.69	1.43
115	559.88	1.6		115	559.74	1.51
116	564.58	1.5		116	564.74	1.49
117	569.88	1.5		117	569.69	1.46
118	574.84	1.6		118	574.84	1.56
119	579.79	1.59				
120	584.88	1.64		120	584.84	1.55
121	589.88	1.63		121	589.69	1.6
122	594.53	1.66		122	594.64	1.67
123	599.83	1.7		123	599.74	1.69
124	604.69	1.73		124	604.79	1.71
125	609.74	1.66		125	609.69	1.6
126	614.84	1.69		126	614.64	1.74
127	619.79	1.72		127	619.74	1.67
128	624.79	1.7				
129	629.83	1.82		129	629.64	1.71
130	634.83	1.61		130	634.74	1.36
131	639.83	1.65		131	639.79	1.54
132	644.88	1.57		132	644.89	1.43
133	649.88	1.43		133	649.94	1.38
134	654.83	1.52		134	654.79	1.42
135	659.79	1.56		135	659.79	1.52
136	664.84	1.72		136	664.79	1.8
137	669.74	1.77		137	669.68	1.82
138	674.79	1.66		138	674.79	1.71
139	679.94	1.69		139	679.79	1.7
140	684.94	1.69		140	684.74	1.69
141	689.89	1.72		141	689.79	1.73
142	694.89	1.69				
143	699.94	1.51		143	699.89	1.64
144	704.92	1.48				
145	709.89	1.44		145	709.79	1.47
146	714.84	1.68		146	714.74	1.76
147	719.69	1.69		147	719.79	1.75
148	724.74	1.77		148	724.79	1.77
149	729.78	1.71		149	729.83	1.76
150	734.78	1.83				
151	739.71	1.9		151	739.68	1.94
152	744.66	1.91		152	744.64	1.94
153	749.74	1.93		153	749.73	1.96
154	754.64	1.96		154	754.64	1.98
155	759.68	1.96		155	759.68	1.98
156	764.67	1.93		156	764.68	1.95
157	769.77	1.9		157	769.79	1.91
158	775.16	1.9		158	775.19	1.91
159	779.6	2.04		159	779.64	2.04
160	784.68	1.88		160	784.73	1.88
161	789.64	1.89		161	789.69	1.89
162	794.78	1.86				
163	799.78	1.85		163	799.84	1.86
164	804.73	1.89		164	804.79	1.9
165	809.58	1.92		165	809.64	1.93
166	814.77	1.9		166	814.84	1.92
167	819.62	1.94		167	819.69	1.96
168	824.62	2.01		168	824.69	2.03
169	829.5	2.08		169	829.58	2.1
170	834.61	2		170	834.69	2.02
171	839.65	1.92		171	839.73	1.95
172	844.6	1.95		172	844.69	1.98

173	849.64	1.97		173	849.73	2
174	854.45	1.94		174	854.54	1.97
175	859.49	2		175	859.58	2.04
176	864.43	2.11		176	864.53	2.15
177	869.43	2.14		177	869.53	2.18
178	874.49	2.03		178	874.59	2.08
179	879.53	1.97		179	879.64	2.02
180	884.53	2.01		180	884.64	2.06
181	889.57	1.97		181	889.68	2.03
182	894.43	2.05		182	894.54	2.11
183	899.62	2		183	899.74	2.07
184	904.57	2.08		184	904.69	2.15
185	909.47	2.08		185	909.59	2.16
186	914.42	2.06		186	914.54	2.15
187	919.57	2.07		187	919.69	2.16
188	924.46	2.11		188	924.59	2.21
189	929.46	2.17		189	929.59	2.27
190	934.46	2.14		190	934.59	2.25
191	939.46	2.13		191	939.59	2.25
192	944.46	2.07		192	944.59	2.19
193	949.34	2.15		193	949.48	2.28
194	954.49	2.19		194	954.63	2.32
195	959.45	2.22		195	959.59	2.36
196	964.2	2.28		196	964.34	2.43
197	969.4	2.22		197	969.54	2.37
198	974.14	2.11		198	974.29	2.27
199	979.24	2.13		199	979.39	2.29
200	984.49	2.23		200	984.64	2.4
201	989.46	2.3		201	989.59	2.47
202	994.57	2.23		202	994.69	2.39
203	999.49	2.2		203	999.59	2.36
204	1004.51	2.2		204	1004.59	2.36
205	1009.38	2.27		205	1009.44	2.42
206	1014.39	2.38		206	1014.44	2.53
207	1019.35	2.4		207	1019.38	2.55
208	1024.53	2.4		208	1024.54	2.54
209	1029.54	2.34		209	1029.54	2.48
210	1034.46	2.35		210	1034.44	2.48
211	1039.27	2.26		211	1039.23	2.39
212	1044.59	2.41		212	1044.54	2.54
213	1049.61	2.53		213	1049.54	2.65
214	1054.63	2.48		214	1054.54	2.6
215	1059.59	2.54		215	1059.49	2.66
216	1064.41	2.56		216	1064.29	2.67
217	1069.73	2.59		217	1069.59	2.7
218	1074.65	2.57		218	1074.49	2.68
219	1079.71	2.66		219	1079.54	2.76
220	1084.48	2.73		220	1084.29	2.83
221	1089.68	2.76		221	1089.53	2.82
222	1094.49	2.52		222	1094.38	2.53
223	1099.56	2.57		223	1099.49	2.54
224	1104.46	2.67		224	1104.44	2.6
225	1109.57	2.72		225	1109.59	2.61
226	1114.23	2.72		226	1114.29	2.56
227	1119.29	2.83		227	1119.39	2.63
228	1124.19	3.17		228	1124.34	2.91
229	1129.14	3.32				
230	1134.19	3.46				
231	1139.04	3.07				
232	1144.24	3.17				
233	1149.19	3.07				
234	1150.33	4.66		234	1150.38	4.67
235	1155.38	4.88		235	1155.54	4.73
236	1160.23	4.53		236	1160.49	4.67
237	1165.18	4.25		237	1165.43	4.5
238	1170.18	4.15		238	1170.29	4.23
239	1175.13	4.05		239	1175.23	4.11
240	1180.13	3.95		240	1180.18	4.05
241	1185.03	3.9		241	1185.08	3.96
242	1190.03	3.95		242	1190.08	4.01

243	1195.12	3.96		243	1195.18	4.02
244	1200.02	4.18		244	1200.08	4.24
245	1204.96	4.4		245	1205.03	4.46
246	1209.96	4.26		246	1210.03	4.33
247	1214.7	4.07		247	1214.78	4.14
248	1219.85	3.98		248	1219.93	4.05
249	1224.59	4.04		249	1224.68	4.11
250	1229.64	4.11		250	1229.73	4.18
251	1234.68	4.1		251	1234.77	4.17
252	1239.57	4.1		252	1239.67	4.17
253	1244.47	4.08		253	1244.57	4.15
254	1249.56	4.07		254	1249.67	4.14
255	1254.46	4.11		255	1254.57	4.18
256	1259.26	4.03		256	1259.38	4.11
257	1264.41	3.94		257	1264.53	4.02
258	1269.3	3.97		258	1269.43	4.05
259	1274.19	3.96		259	1274.32	4.04
260	1279.18	4.02		260	1279.32	4.1
261	1284.13	3.95		261	1284.27	4.03
262	1289.15	4.04		262	1289.28	4.13
263	1293.89	4.05		263	1294.02	4.14
264	1299	4.03		264	1299.12	4.13
265	1303.85	3.99		265	1303.97	4.1
266	1308.91	3.98		266	1309.02	4.09
267	1313.81	4.04		267	1313.92	4.16
268	1318.82	4.06		268	1318.92	4.19
269	1323.81	3.89		269	1323.91	4.03
270	1328.68	3.89		270	1328.77	4.03
271	1333.74	3.85		271	1333.82	4
272	1338.64	4.02		272	1338.72	4.18
273	1343.65	3.98		273	1343.72	4.14
274	1348.75	4.03		274	1348.82	4.2
275	1353.51	4.04		275	1353.57	4.22
276	1358.61	4.17		276	1358.67	4.35
277	1363.36	4.08		277	1363.41	4.27
278	1368.31	4.1		278	1368.36	4.29
279	1373.26	4.12		279	1373.46	4.35
280	1378.37	4.23		280	1378.42	4.4
281	1383.31	4.23		281	1383.36	4.46
282	1388.26	4.24		282	1388.51	4.42
283	1392.97	4.29		283	1393.21	4.47
284	1398.08	4.3		284	1398.31	4.49
285	1403.09	4.38		285	1403.31	4.57
286	1408.05	4.37		286	1408.26	4.56
287	1412.96	4.33		287	1413.16	4.53
288	1417.97	4.27		288	1418.16	4.47
289	1422.78	4.3		289	1422.96	4.51
290	1427.89	3.41		290	1428.06	3.62
291	1432.75	4.39		291	1432.91	4.6
292	1437.82	4.35		292	1437.96	4.57
293	1442.73	4.35		293	1442.86	4.57
294	1447.74	4.37		294	1447.86	4.59
295	1452.6	4.3		295	1452.71	4.53
296	1457.61	4.29		296	1457.71	4.52
297	1462.67	4.31		297	1462.76	4.55
298	1467.63	4.39		298	1467.71	4.63
299	1472.54	4.44		299	1472.61	4.68
300	1477.54	4.38		300	1477.6	4.63
301	1482.6	4.51		301	1482.65	4.76
302	1487.51	4.73		302	1487.61	4.84
303	1492.41	5.12		303	1492.56	5.08
304	1497.3	5.4		304	1497.5	5.22
305	1502.2	5.07		305	1502.5	5.38
306	1507.1	4.58		306	1507.4	4.89
307	1511.91	4.65		307	1512.2	4.96
308	1516.86	4.63		308	1517.15	4.94
309	1521.92	4.69		309	1522.21	5
310	1526.92	4.62		310	1527.2	4.93
311	1531.92	4.63		311	1532.2	4.94
312	1536.77	4.72		312	1537.05	5.03

313	1541.82	4.57		313	1542.1	4.87
314	1546.73	4.53		314	1547	4.83
315	1551.68	4.59		315	1551.95	4.89
316	1556.57	4.63		316	1556.84	4.93
317	1561.68	4.59		317	1561.94	4.89
318	1566.53	4.6		318	1566.79	4.9
319	1571.54	4.61		319	1571.8	4.91
320	1576.5	4.53		320	1576.75	4.83
321	1581.4	4.57		321	1581.65	4.87
322	1586.31	4.56		322	1586.55	4.86
323	1591.27	4.59		323	1591.5	4.89
324	1596.07	4.6		324	1596.29	4.9
325	1601.14	4.61		325	1601.35	4.91
326	1606.14	4.59		326	1606.34	4.89
327	1610.95	4.59		327	1611.14	4.89
328	1616.01	4.62		328	1616.19	4.92
329	1620.98	4.67		329	1621.15	4.97
330	1626.09	4.63		330	1626.25	4.93
331	1630.89	4.58		331	1631.04	4.88
332	1635.8	4.61		332	1635.94	4.91
333	1640.86	4.59		333	1640.99	4.89
334	1645.77	4.68		334	1645.89	4.98
335	1650.87	4.66		335	1650.98	4.96
336	1655.69	4.64		336	1655.79	4.94
337	1660.7	4.73		337	1660.79	5.03
338	1665.5	4.77		338	1665.58	5.07
339	1670.52	4.76		339	1670.59	5.06
340	1675.58	4.72		340	1675.64	5.02
341	1680.49	4.72		341	1680.54	5.02
342	1685.43	4.68		342	1685.49	4.98
343	1690.4	4.74		343	1690.48	5.05
344	1695.24	4.83		344	1695.33	5.14
345	1700.08	4.67		345	1700.18	4.99
346	1705.23	4.69		346	1705.34	5.01
347	1710.01	4.72		347	1710.13	5.05
348	1714.89	4.77		348	1715.03	5.1
349	1719.93	4.69		349	1720.08	5.03
350	1724.87	4.76		350	1725.03	5.1
351	1730.01	4.77		351	1730.18	5.11
352	1734.79	4.78		352	1734.98	5.13
353	1739.63	4.56		353	1739.83	4.91
354	1744.77	4.74		354	1744.98	5.1
355	1749.7	4.72		355	1749.93	5.08
356	1754.64	4.89		356	1754.88	5.26
357	1759.43	4.86		357	1759.68	5.23
358	1764.37	4.83		358	1764.63	5.21
359	1769.3	4.93		359	1769.58	5.31
360	1774.39	4.98		360	1774.68	5.37
361	1779.33	5.03		361	1779.63	5.42
362	1784.17	5.24		362	1784.48	5.63
363	1789.2	5.35		363	1789.52	5.74
364	1794.14	5.33				
365	1799.09	5.24		365	1799.43	5.63
366	1804.18	5.13		366	1804.53	5.52
367	1808.96	5.1		367	1809.32	5.49
368	1813.86	5.06		368	1814.23	5.45
369	1818.84	5.07		369	1819.22	5.46
370	1823.83	4.95		370	1824.22	5.34
371	1828.77	4.99		371	1829.17	5.38
372	1833.75	4.9		372	1834.17	5.3
373	1838.49	4.96		373	1838.92	5.36
374	1843.23	4.98		374	1843.67	5.38
375	1848.22	4.99		375	1848.67	5.39
376	1853.11	4.95		376	1853.57	5.35
377	1858.1	4.96		377	1858.57	5.36
378	1863.24	5.09		378	1863.72	5.49
379	1868.13	5.09		379	1868.62	5.49
380	1873.12	5.15		380	1873.62	5.55
381	1878.06	5.14		381	1878.57	5.54
382	1883.09	5.09		382	1883.57	5.49

383	1888	5.13		383	1888.46	5.53
384	1892.98	5.08		384	1893.41	5.48
385	1898.02	5.04		385	1898.42	5.44
386	1903.13	5.06		386	1903.51	5.47
387	1907.96	4.97		387	1908.31	5.38
388	1913.05	5.03		388	1913.37	5.44
389	1917.96	5.02		389	1918.26	5.43
390	1922.84	5.08		390	1923.11	5.49
391	1927.53	5.16				
392	1933.11	5.25		392	1933.32	5.66
393	1937.93	5.22		393	1938.12	5.63
394	1943.01	5.19		394	1943.17	5.6
395	1947.98	5.36		395	1948.11	5.77
396	1953.11	5.2		396	1953.22	5.62
397	1958.18	5.14		397	1958.26	5.56
398	1963.31	5.13		398	1963.36	5.55
399	1968.28	5.16		399	1968.31	5.58
400	1973.16	5.25		400	1973.16	5.67
401	1978.15	5.21		401	1978.16	5.62
402	1983.1	5.11		402	1983.12	5.52
403	1988.09	5.11		403	1988.11	5.51
404	1993.08	5.17		404	1993.11	5.56
405	1998.02	5.16		405	1998.06	5.54
406	2003.07	5.14		406	2003.11	5.51
407	2008.06	5.11		407	2008.11	5.48
408	2013.16	5.12		408	2013.22	5.48
409	2018.14	5.1		409	2018.21	5.45
410	2023.14	5.22		410	2023.21	5.56
411	2028.18	5.18		411	2028.26	5.52
412	2033.12	5.2		412	2033.21	5.53
413	2038.11	5.27		413	2038.21	5.59
414	2042.96	5.26		414	2043.06	5.57
415	2048	5.16		415	2048.11	5.47
416	2053.24	5.14				
417	2058.23	5.15		417	2058.36	5.44
418	2063.32	5.25		418	2063.46	5.53
419	2068.27	5.21		419	2068.41	5.49
420	2073.26	5.23		420	2073.41	5.5
421	2078.31	5.19		421	2078.46	5.46
422	2083.2	5.2		422	2083.36	5.48
423	2088.24	5.24		423	2088.41	5.52
424	2093.39	5.17		424	2093.56	5.46
425	2098.14	5.16		425	2098.31	5.45
426	2103.19	5.17		426	2103.37	5.46
427	2108.23	5.2		427	2108.41	5.5
428	2113.12	5.23		428	2113.31	5.53
429	2118.06	5.3				
430	2123.11	5.13		430	2123.31	5.44
431	2128.21	5.14		431	2128.41	5.45
432	2133.15	5.12		432	2133.36	5.44
433	2138.25	5.14		433	2138.46	5.46
434	2142.94	5.31		434	2143.16	5.64
435	2148.04	5.4		435	2148.26	5.73
436	2153.18	5.18		436	2153.41	5.51
437	2157.98	5.38		437	2158.21	5.72
438	2162.97	5.42		438	2163.21	5.76
439	2168.02	5.44		439	2168.27	5.79
440	2173.01	5.49		440	2173.26	5.84
441	2177.92	5.51		441	2178.11	5.87
442	2182.88	5.48		442	2183.01	5.84
443	2187.59	5.64		443	2187.67	6.01
444	2192.65	5.62		444	2192.67	5.99
445	2197.45	5.62		445	2197.41	6
446	2202.67	5.64		446	2202.57	6.02
447	2207.12	5.66		447	2206.97	6.05
448	2211.98	5.65		448	2211.77	6.04
449	2216.49	5.74		449	2216.22	6.14
450	2221.09	5.8		450	2220.77	6.21
451	2225.65	5.73		451	2225.27	6.14
452	2229.96	5.72		452	2229.52	6.14

453	2234.77	5.72		453	2234.27	6.14
454	2238.64	5.68		454	2238.08	6.11
455	2242.74	5.61		455	2242.13	6.04
456	2246.61	5.84		456	2245.94	6.28
457	2250.57	5.55				
458	2254.51	5.8		458	2253.73	6.25
459	2258.18	5.81		459	2257.34	6.26
460	2261.99	5.71		460	2261.09	6.17
461	2266.07	5.57		461	2265.19	6.01
462	2269.76	5.56		462	2268.9	5.98
463	2273.35	5.5		463	2272.5	5.91
464	2276.78	5.56		464	2275.95	5.95
465	2280.56	5.35		465	2279.75	5.72
466	2284	5.46		466	2283.21	5.81
467	2287.74	5.25		467	2286.96	5.58
468	2291.57	5.3		468	2290.81	5.62
469	2295.36	5.37				
470	2298.94	5.62		470	2298.21	5.9
471	2302.83	5.63		471	2302.12	5.89
472	2306.76	5.7		472	2306.07	5.94
473	2310.84	5.7		473	2310.17	5.93
474	2314.98	5.72				
475	2319.26	5.79				
476	2323.74	5.68		476	2323.12	5.85
477	2328.13	5.79		477	2327.53	5.94
478	2332.81	5.86		478	2332.23	6
479	2337.3	5.89		479	2336.73	6.01
480	2341.78	5.98		480	2341.23	6.08
481	2346.61	5.95		481	2346.08	6.05
482	2351.4	5.97		482	2350.89	6.06
483	2356.12	5.99		483	2355.63	6.08
484	2361.01	5.99		484	2360.54	6.08
485	2366.23	6.04		485	2365.78	6.13
486	2370.92	6.14		486	2370.49	6.23
487	2376.09	6.28		487	2375.68	6.36
488	2381.13	6.2		488	2380.74	6.28
489	2386.16	6.29		489	2385.79	6.37
490	2391.29	6.24		490	2390.94	6.31
491	2396.03	6.26		491	2395.69	6.33
492	2401.01	6.4		492	2400.69	6.47
493	2405.94	6.49				
494	2411.12	6.53				
495	2415.95	6.55		495	2415.69	6.61
496	2420.98	6.58				
497	2425.81	6.58		497	2425.59	6.64
498	2430.84	6.55		498	2430.64	6.6
499	2435.97	6.54		499	2435.79	6.59
500	2440.79	6.57		500	2440.63	6.62
501	2445.78	6.61		501	2445.64	6.65
502	2450.77	6.71		502	2450.64	6.75
503	2455.65	6.66		503	2455.54	6.69
504	2460.79	6.6		504	2460.69	6.63
505	2465.77	6.5		505	2465.69	6.52
506	2470.61	6.47				
507	2475.74	6.39		507	2475.69	6.4
508	2480.63	6.19		508	2480.59	6.19
509	2485.61	6.06		509	2485.59	6.06
510	2490.65	5.92		510	2490.64	5.91
511	2495.58	5.82		511	2495.59	5.8
512	2500.56	5.77		512	2500.59	5.75
513	2505.5	5.8		513	2505.54	5.77
514	2510.58	5.83				
515	2515.62	5.9		515	2515.69	5.86
516	2520.6	5.93		516	2520.69	5.88
517	2525.49	5.91		517	2525.59	5.86
518	2530.43	6.03		518	2530.55	5.97
519	2535.46	6.04		519	2535.59	5.98
520	2540.44	6.05		520	2540.59	5.98
521	2545.21	6.06		521	2545.34	6
522	2550.33	6.08		522	2550.44	6.03

523	2555.27	6.06		523	2555.35	6.02
524	2560.38	6.15		524	2560.44	6.12
525	2565.45	6.39		525	2565.49	6.37
526	2569.72	6.67		526	2569.74	6.66
527	2574.55	6.94		527	2574.54	6.94
528	2579.13	7.02		528	2579.1	7.03
529	2584.05	7.06		529	2584	7.08
530	2588.72	7.07		530	2588.65	7.1
531	2593.65	7.08		531	2593.55	7.12
532	2598.17	7.12		532	2598.05	7.17
533	2602.89	7.1		533	2602.75	7.16
534	2607.73	7.05		534	2607.56	7.12
535	2612.29	7.14		535	2612.1	7.22
536	2617.07	7.16		536	2616.86	7.25
537	2621.69	7.14		537	2621.46	7.24
538	2626.26	7.19		538	2626	7.3
539	2630.54	7.05		539	2630.26	7.17
540	2635.76	7.17		540	2635.46	7.3
541	2640.3	7.14		541	2640.01	7.27
542	2645.09	7.22				
543	2649.77	7.16		543	2649.51	7.29
544	2654.61	7.16		544	2654.36	7.29
545	2659.15	7.22		545	2658.91	7.34
546	2663.85	7.18		546	2663.62	7.3
547	2668.68	7.22		547	2668.47	7.34
548	2673.17	7.19		548	2672.97	7.31
549	2677.96	7.22		549	2677.77	7.34
550	2682.59	7.24		550	2682.42	7.36
551	2687.18	7.24		551	2687.02	7.36
552	2691.88	7.28		552	2691.73	7.4
553	2696.67	7.29		553	2696.53	7.41
554	2701.41	7.36		554	2701.28	7.48
555	2705.99	7.38		555	2705.88	7.5
556	2710.73	7.41		556	2710.63	7.52
557	2715.52	7.44		557	2715.43	7.55
558	2720.66	7.46		558	2720.58	7.57
559	2725.39	7.47		559	2725.33	7.58
560	2730.43	7.45		560	2730.38	7.56
561	2735.41	7.47		561	2735.38	7.55
562	2740.34	7.47		562	2740.33	7.51
563	2745.43	7.47		563	2745.44	7.48
564	2750.36	7.52		564	2750.38	7.5
565	2755.29	7.56		565	2755.33	7.5
566	2760.32	7.55		566	2760.38	7.46
567	2765.25	7.45		567	2765.33	7.33
568	2769.98	7.45		568	2770.08	7.29
569	2774.91	7.44		569	2775.03	7.25
570	2779.74	7.53		570	2779.87	7.31
571	2784.63	7.58		571	2784.78	7.33
572	2789.41	7.74		572	2789.58	7.45
573	2794.19	7.81		573	2794.38	7.49
574	2799.12	7.95		574	2799.33	7.6
575	2803.94	7.98		575	2804.17	7.59
576	2808.73	8.04		576	2808.97	7.62
577	2813.61	8.16		577	2813.87	7.71
578	2818.49	8				
579	2823.32	7.64		579	2823.62	7.12
580	2828.32	7.41		580	2828.42	7.07
581	2833.17	7.66		581	2833.12	7.18

Appendix C

Distances and elevations along East Bay Seismic Profile 2 (SL-2).
Measurements are relative to the first receiver point at the west end of Profile SL-2.

Station No.	Receiver Dist. (m)	Receiver Elev. (m)		Station No.	Shot Dist. (m)	Shot Elev. (m)
1	0	2.15		1	0	2.15
2	5.05	1.63		2	5.05	1.63

3	9.83	1.2		3	9.83	1.2
4	14.6	0.75		4	14.6	0.75
5	19.23	0.44		5	19.23	0.44
6	24.05	0.34		6	24.05	0.34
7	28.63	0.32		7	28.63	0.32
8	33.51	0.29		8	33.51	0.29
9	38.11	0.27		9	38.11	0.27
10	42.57	0.22		10	42.57	0.22
11	47.04	0.16		11	47.04	0.16
12	51.55	0.18		12	51.55	0.18
13	55.96	0.13		13	55.96	0.13
14	60.49	0.11				
15	65	0.18		15	65	0.18
16	69.47	0.17		16	69.47	0.17
17	73.92	0.17		17	73.92	0.17
18	78.33	0.17		18	78.33	0.17
19	82.86	0.18		19	82.86	0.18
20	87.39	0.19		20	87.39	0.19
21	91.92	0.2		21	91.92	0.2
22	96.45	0.2		22	96.45	0.2
23	100.86	0.19		23	100.86	0.19
24	105.3	0.18		24	105.3	0.18
25	109.76	0.15		25	109.76	0.15
26	114.22	0.14		26	114.22	0.14
27	118.88	0.12		27	118.88	0.12
28	123.55	0.08		28	123.55	0.08
29	128.71	0.13		29	128.71	0.13
30	133.35	0.14		30	133.35	0.14
31	138.36	0.18		31	138.36	0.18
32	143.24	0.29		32	143.24	0.29
33	148.14	0.26		33	148.14	0.26
34	153.17	0.4		34	153.17	0.4
35	158.28	0.46		35	158.28	0.46
36	163.18	0.46				
37	168.26	0.47		37	168.26	0.47
38	173.29	0.55		38	173.29	0.55
39	178.28	0.49		39	178.28	0.49
40	183.23	0.53		40	183.23	0.53
41	188.17	0.6		41	188.17	0.6
42	193.31	0.65		42	193.31	0.65
43	198.2	0.69		43	198.2	0.69
44	203.22	0.57		44	203.22	0.57
45	208.37	0.6		45	208.37	0.6
46	213.13	0.65		46	213.13	0.65
47	218.22	0.69		47	218.22	0.69
48	223.16	0.66		48	223.16	0.66
49	228.23	0.72		49	228.23	0.72
50	233.25	0.76		50	233.25	0.76
51	238.13	0.8				
52	243.15	0.7		52	243.15	0.7
53	248.03	0.8		53	248.03	0.8
54	253.04	0.87		54	253.04	0.87
55	258.04	0.85		55	258.04	0.85
56	263.11	0.75		56	263.11	0.75
57	268.02	0.93		57	268.02	0.93
58	272.99	0.82		58	272.99	0.82
59	277.98	0.92		59	277.98	0.92
60	283.27	1.03		60	283.27	1.03
61	288.09	1.03		61	288.09	1.03
62	293.11	1.01		62	293.11	1.01
63	298.08	1.02		63	298.08	1.02
64	302.9	1.03		64	302.9	1.03
65	307.56	1.02		65	307.56	1.02
66	312.39	0.76		66	312.39	0.76
67	317.54	0.74		67	317.54	0.74
68	322.37	0.91		68	322.37	0.91
69	327.34	0.94		69	327.34	0.94
70	332.19	0.96		70	332.19	0.96
71	337.05	0.94		71	337.05	0.94
72	342.27	0.97		72	342.27	0.97

73	347.28	0.91		73	347.28	0.91
74	352.31	0.9		74	352.31	0.9
75	357.27	0.92		75	357.27	0.92
76	362.16	0.86		76	362.16	0.86
77	367.07	0.83		77	367.07	0.83
78	372.13	0.78		78	372.13	0.78
79	377.12	0.74		79	377.12	0.74
80	382.12	0.77		80	382.12	0.77
81	387.06	0.8		81	387.06	0.8
82	391.98	0.77		82	391.98	0.77
83	396.61	0.64		83	396.61	0.64
84	401.26	1.06		84	401.26	1.06
85	405.72	1.07		85	405.72	1.07
86	409.81	1.11		86	409.81	1.11
87	414.04	1.03		87	414.04	1.03
88	417.98	1.19		88	417.98	1.19
89	422	1.18		89	422	1.18
90	426.29	1.21		90	426.29	1.21
91	429.87	1.22		91	429.87	1.22
92	434.1	1.24		92	434.1	1.24
93	438.4	1.63		93	438.4	1.63
94	442.56	1.67		94	442.56	1.67
95	446.86	1.79		95	446.86	1.79
96	451.15	1.84		96	451.15	1.84
97	455.59	1.87		97	455.59	1.87
98	460.1	1.82		98	460.1	1.82
99	464.68	1.93		99	464.68	1.93
100	469.57	1.88		100	469.57	1.88
101	474.5	1.91		101	474.5	1.91
102	479.4	1.93		102	479.4	1.93
103	484.34	1.92		103	484.34	1.92
104	489.22	1.86		104	489.22	1.86
105	494.28	1.85		105	494.28	1.85
106	499.22	1.79		106	499.22	1.79
107	504.16	1.83		107	504.16	1.83
108	509.23	1.75		108	509.23	1.75
109	514.21	1.8		109	514.21	1.8
110	519.04	1.9		110	519.04	1.9
111	524.03	1.87		111	524.03	1.87
112	529.02	1.87		112	529.02	1.87
113	533.91	1.91		113	533.91	1.91
114	538.96	1.89		114	538.96	1.89
115	543.81	1.9		115	543.81	1.9
116	548.68	1.84		116	548.68	1.84
117	553.8	1.89		117	553.8	1.89
118	558.67	1.89		118	558.67	1.89
119	563.72	1.99		119	563.72	1.99
120	568.57	2.02				
121	573.51	2		121	573.51	2
122	578.68	2		122	578.68	2
123	583.61	2.19		123	583.61	2.19
124	588.62	2.2		124	588.62	2.2
125	593.47	2.28		125	593.47	2.28
126	598.64	2.33		126	598.64	2.33
127	603.52	2.34		127	603.52	2.34
128	608.67	2.5		128	608.67	2.5
129	613.6	2.56		129	613.6	2.56
130	618.56	2.55		130	618.56	2.55
131	623.46	2.47		131	623.46	2.47
132	628.24	2.46		132	628.24	2.46
133	632.94	2.54		133	632.94	2.54
134	637.57	2.44		134	637.57	2.44
135	642.1	2.51		135	642.1	2.51
136	646.7	2.42		136	646.7	2.42
137	651.19	2.43		137	651.19	2.43
138	655.34	2.42		138	655.34	2.42
139	659.49	2.43		139	659.49	2.43
140	663.18	2.48		140	663.18	2.48
141	666.74	2.42		141	666.74	2.42
142	670.55	2.44		142	670.55	2.44

143	673.48	2.56	143	673.48	2.56
144	677.08	2.81			
145	680.76	3.47	145	680.76	3.47
146	684.11	3.6	146	684.11	3.6
147	687.5	3.7	147	687.5	3.7
148	691.15	3.77	148	691.15	3.77
149	694.31	3.81	149	694.31	3.81
150	697.77	3.81	150	697.77	3.81
151	701.18	3.81	151	701.18	3.81
152	704.84	3.77	152	704.84	3.77
153	708.34	3.85	153	708.34	3.85
154	711.94	3.9			
155	715.36	3.86			
156	718.86	3.86			
157	722.36	3.86			
158	725.86	3.86			
159	729.36	3.86			

Appendix D

Distances and elevations along East Bay Seismic Profile 3 (SL-3).
Measurements are relative to the first shotpoint at the west end of Profile SL-3.

Station No.	Receiver Dist. (m)	Receiver Elev. (m)	Station No.	Shot Dist. (m)	Shot Elev. (m)
1	0.22	0.04	1	0	0.41
2	5.29	0.2	2	5.05	0.56
3	10.09	0.24	3	9.84	0.59
4	14.87	0.23	4	14.6	0.58
5	19.82	0.23	5	19.54	0.57
6	24.86	0.26	6	24.56	0.59
7	29.79	0.12			
8	34.52	0.25	8	34.19	0.56
9	39.65	0.15	9	39.31	0.45
10	44.44	0.19	10	44.08	0.49
11	49.4	0			
12	54.03	0.09	12	53.64	0.37
13	58.84	0.22	13	58.44	0.49
14	63.13	0.49	14	62.71	0.75
15	67.45	0.49	15	67.02	0.75
16	72.03	0.61	16	71.58	0.86
17	76.74	0.6	17	76.28	0.84
18	81.14	0.51	18	80.66	0.74
19	85.77	0.44	19	85.28	0.66
20	90.24	0.35	20	89.73	0.57
21	94.63	0.43	21	94.11	0.64
22	99.28	0.52	22	98.74	0.72
23	103.68	0.65	23	103.13	0.84
24	108.21	0.68	24	107.64	0.86
25	112.61	1.11	25	112.03	1.28
26	116.62	1.66	26	116.02	1.83
27	121.08	2.16	27	120.47	2.32
28	125.73	2.15	28	125.1	2.3
29	130.29	1.71	29	130.2	1.99
30	135.05	1.24	30	135.2	1.33
31	140	1.02	31	140.17	1.15
32	144.99	1.03	32	145.02	1.18
33	149.96	1.03	33	149.8	1.2
34	154.85	1.04	34	154.76	1.19
35	159.85	1.02	35	159.88	1.11
36	164.55	0.99	36	164.64	1.12
37	169.66	1.03			
38	174.34	0.94	38	174.44	1.17
39	178.88	0.96	39	179.27	1.03
40	183.66	0.8	40	183.94	0.98
41	188.16	0.89	41	188.49	0.97
42	192.56	0.86	42	192.83	1.03
43	197.1	0.79	43	197.37	0.95
44	201.57	1	44	201.9	0.98

45	205.96	1.24		45	206.25	1.24
46	210.51	1		46	210.77	1.02
47	215.09	1.04		47	215.31	1.08
48	219.53	0.94		48	219.72	1
49	223.99	0.88		49	224.14	0.96
50	228.68	0.69		50	228.8	0.79
51	233.22	0.54		51	233.3	0.66
52	238.04	0.75		52	238.09	0.89
53	242.9	0.47		53	242.91	0.63
54	247.98	0.52		54	247.96	0.7
55	252.85	0.54		55	252.8	0.74
56	257.79	0.53		56	257.7	0.75
57	263.07	0.61		57	262.74	0.79
58	267.89	0.6		58	267.56	0.79
59	272.85	0.79		59	272.56	0.83
60	277.68	0.88		60	277.28	0.88
61	282.54	0.82		61	281.96	0.9
62	286.84	1.08		62	286.21	0.93
63	291.56	0.9		63	290.97	1.1
64	296.01	0.97		64	295.37	1.27
65	300.35	1.03		65	299.64	1.39
66	304.71	1.04		66	304.03	1.36
67	308.8	1.03		67	308.14	1.32
68	312.87	1.12		68	312.24	1.37
69	317.2	1.34		69	316.6	1.55
70	321.43	1.31		70	320.86	1.48
71	325.63	1.45		71	325.08	1.59
72	329.83	1.5		72	329.31	1.6
73	334.23	1.59		73	333.53	1.66
74	338.5	1.66		74	337.86	1.84
75	343.01	1.71		75	342.48	1.88
76	347.57	1.71		76	347.17	1.82
77	352.3	1.75		77	352.03	1.85
78	357.09	1.76		78	356.76	1.87
79	361.86	1.78		79	361.65	1.83
80	366.71	1.82		80	366.53	1.92
81	371.8	1.82		81	371.64	1.96
82	376.66	1.84		82	376.64	1.98
83	381.58	1.84		83	381.56	1.95
84	386.48	1.77				
85	391.43	1.82				
86	396.32	1.83		86	396.34	1.92
87	400.92	2.04				
88	405.54	2.13		88	405.76	2.23
89	409.76	1.76		89	410	1.87
90	414.28	1.59				
91	419.32	1.61		91	419.58	1.74
92	423.59	1.6				
93	428.17	1.56		93	428.46	1.71
94	433.07	1.56				
95	437.6	1.49				
96	442.05	1.54		96	442.38	1.72
97	446.33	1.59		97	446.67	1.78
98	450.93	1.6		98	451.39	1.72
99	455.53	1.56				
100	460.07	1.51		100	460.53	1.68
101	464.55	1.49		101	465	1.61
102	469.27	1.46		102	469.61	1.58
103	474.25	1.42		103	474.59	1.62
104	478.99	1.41		104	479.21	1.61
105	484	1.49		105	483.96	1.58
106	488.97	1.47		106	488.91	1.57
107	493.99	1.67		107	493.92	1.78
108	499.05	1.66		108	498.96	1.78
109	504.08	1.72		109	503.98	1.85
110	509.12	1.83		110	509	1.97
111	514.04	1.81		111	513.9	1.96
112	519.33	1.79		112	519.18	1.95
113	524.19	1.88		113	524.02	2.05
114	529.17	1.94		114	528.99	2.12

115	534.95	2.02	115	534.75	2.21
116	538.7	2.06	116	538.92	2.14
117	543.78	2.15	117	543.46	2.21
118	548.12	2.19	118	548.4	2.31
119	553.42	2.14			
120	558.36	2.13			
121	562.8	2.06			
122	567.65	2.06	122	567.94	2.21
123	572.63	2.03	123	572.87	2.18
124	577.3	2.05	124	577.49	2.19
125	582.34	2.04	125	582.48	2.18
126	587.01	2.05	126	587.1	2.19
127	591.5	2.25	127	591.54	2.39
128	596.12	2.34	128	596.52	2.59
129	600.92	2.38	129	601.08	2.57
130	605.84	2.37	130	606.19	2.59
131	610.59	2.48	131	610.93	2.46
132	615.22	2.36	132	615.56	2.35
133	620.19	2.3	133	620.53	2.3
134	625.06	2.31	134	625.4	2.33
135	629.63	2.24	135	629.96	2.27
136	634.38	2.24	136	634.71	2.28
137	639.24	2.2	137	639.57	2.25
138	643.85	2.16	138	644.18	2.23
139	648.96	2.24	139	649.29	2.32
140	653.75	2.31	140	654.09	2.3
141	658.15	2.29	141	658.46	2.28
142	663.35	2.43	142	663.63	2.42
143	667.95	2.46	143	668.19	2.46
144	672.73	2.41	144	672.94	2.41

Appendix E

Distances and elevations along East Bay Seismic Profile 4 (SL-4).
Measurements are relative to the first receiver point at the west end of Profile SL-4.

Station No.	Receiver Dist. (m)	Receiver Elev. (m)	Station No.	Shot Dist. (m)	Shot Elev. (m)
1	0	0.99			
2	5.07	1.39	2	5.21	1.22
3	10.56	1.2	3	10.27	1.22
4	15.21	1.12	4	14.91	1.15
5	20.16	1.12			
6	25.15	1.19			
7	30.1	1.08			
8	35.13	1.07			
9	40.17	1.17			
10	44.99	1.29			
11	50.02	1.3			
12	55.16	1.38			
13	60.02	1.47			
14	65.06	1.52			
15	70.19	1.56			
16	75.01	1.59			
17	80	1.52			
18	85.09	1.51			
19	90.08	1.49			
20	95.12	1.4			
21	99.94	1.31			
22	104.98	1.2			
23	110.06	1.19			
24	115.11	1.03			
25	120.01	1.1			
26	125.63	1.14			
27	130.09	1.15			
28	135.13	1.17			
29	140	1.07			
30	145.04	0.98			
31	149.94	0.82			

32	154.98	0.7	32	155	0.63
33	160.07	0.73	33	160.22	0.69
34	164.44	0.76	34	164.46	0.7
35	169.84	0.72	35	170.21	0.7
36	174.92	0.77	36	174.94	0.71
37	179.91	0.72	37	179.97	0.7
38	184.95	0.71	38	184.97	0.67
39	190.25	0.69	39	190.1	0.7
40	194.94	0.68	40	195.05	0.66
41	199.93	0.68	41	199.83	0.67
42	204.88	0.65	42	204.86	0.63
43	209.93	0.63	43	210.04	0.62
44	214.92	0.56	44	214.9	0.51
45	219.95	0.57	45	219.71	0.54
46	224.82	0.55	46	225.15	0.58
47	230.26	0.55	47	230.2	0.56
48	234.9	0.57	48	235.02	0.56
49	239.89	0.55	49	240.09	0.55
50	244.89	0.56	50	244.96	0.55
51	249.88	0.64	51	249.96	0.62
52	254.92	0.65	52	254.72	0.63
53	259.92	0.56	53	259.85	0.52
54	264.95	0.37	54	264.97	0.5
55	269.91	0.48			

Appendix F

Distances and elevations along East Bay Seismic Profile 5 (SL-5).
Measurements are relative to the first receiver point at the west end of Profile SL-5.

Station No.	Receiver Dist. (m)	Receiver Elev. (m)	Station No.	Shot Dist. (m)	Shot Elev. (m)
1	0.04	0.14			
2	5.05	0.15			
3	9.62	0.3			
4	14.71	0.53			
5	19.04	0.47			
6	24.46	0.44			
7	30.5	0.51			
8	35.04	0.46			
9	40	0.41	9	40.06	0.37
10	44.93	0.37	10	44.86	0.34
11	49.86	0.44	11	49.71	0.41
12	54.87	0.56	12	54.77	0.56
13	59.78	0.69	13	59.84	0.68
14	64.89	0.77	14	64.74	0.76
15	69.95	0.78			
16	74.91	0.79	16	74.87	0.82
17	79.96	0.87	17	79.91	0.89
18	84.98	0.83	18	84.92	0.85
19	89.83	0.89	19	89.83	0.88
20	94.83	0.96			
21	99.84	0.92	21	99.95	0.95
22	104.9	1.04	22	104.96	1.05
23	109.91	1.07	23	110.14	1.1
24	114.87	1.14	24	114.83	1.1
25	119.88	1.16	25	119.9	1.15
26	124.9	1.17	26	124.9	1.15
27	129.95	1.17	27	129.51	1.09
28	135	1.21	28	134.93	1.18
29	139.81	1.22	29	139.82	1.17
30	144.86	1.28	30	144.83	1.26
31	149.87	1.24	31	149.63	1.23
32	154.67	1.23			
33	159.73	1.21	33	159.81	1.17
34	164.74	1.18	34	164.61	1.14
35	169.8	1.13	35	169.81	1.12
36	174.76	1.1	36	174.84	1.03
37	179.86	1.08	37	179.69	1.07

38	184.83	0.99	38	184.79	0.96
39	189.79	0.91	39	189.89	0.9
40	194.87	0.91	40	194.77	0.88
41	199.83	0.88	41	199.68	0.91
42	204.79	0.86	42	204.8	0.9
43	209.8	0.86			
44	214.72	0.83	44	214.68	0.88
45	219.68	0.86	45	219.9	0.85
46	224.85	0.89	46	224.81	0.88
47	229.76	0.88	47	229.68	0.88
48	234.73	0.89	48	234.6	0.86
49	239.64	0.83	49	239.65	0.81
50	244.86	0.77			
51	250.03	0.75			
52	254.8	0.69			
53	259.63	0.65			
54	264.63	0.65	54	264.74	0.64
55	269.48	1.26			
56	274.56	0.87			
57	279.64	0.47			
58	284.38	0.46	58	284.44	0.43

Appendix G

Distances and elevations along East Bay Seismic Profile 6 (SL-6).
Measurements are relative to the first receiver point at the west end of Profile SL-6.

Station No.	Receiver Dist. (m)	Receiver Elev. (m)	Station No.	Shot Dist. (m)	Shot Elev. (m)
1	0	0.07	1	0	0.07
2	5.64	0.17	2	5.64	0.17
3	10.36	0	3	10.36	0
4	15.4	0.05	4	15.4	0.05
5	20.66	0.05	5	20.66	0.05
6	25.52	0.16	6	25.52	0.16
7	30.43	0.17	7	30.43	0.17
8	35.47	0.19	8	35.47	0.19
9	40.51	0.2	9	40.51	0.2
10	45.46	0.25	10	45.46	0.25
11	50.37	0.28	11	50.37	0.28
12	55.54	0.26	12	55.54	0.26
13	60.32	0.32	13	60.32	0.32
14	65.4	0.29	14	65.4	0.29
15	70.53	0.24	15	70.53	0.24
16	75.48	0.07	16	75.48	0.07
17	80.42	0.3	17	80.42	0.3
18	85.45	0.24	18	85.45	0.24
19	90.38	0.17	19	90.38	0.17
20	95.42	0.13	20	95.42	0.13
21	100.42	0.54	21	100.42	0.54
22	105.24	0.16	22	105.24	0.16
23	110.41	0.12	23	110.41	0.12
24	115.36	0.26	24	115.36	0.26
25	120.14	0.21	25	120.14	0.21
26	125.57	0.24	26	125.57	0.24
27	130.35	0.28	27	130.35	0.28
28	134.94	0.29	28	134.94	0.29
29	140.43	0.31	29	140.43	0.31
30	145.33	0.48	30	145.33	0.48
31	150.41	0.34	31	150.41	0.34
32	155.28	0.37	32	155.28	0.37
33	160.24	0.34	33	160.24	0.34
34	165.32	0.4	34	165.32	0.4
35	170.44	0.35	35	170.44	0.35
36	175.42	0.36	36	175.42	0.36
37	180.22	0.37	37	180.22	0.37
38	185.26	0.42	38	185.26	0.42
39	190.3	0.46	39	190.3	0.46
40	195.2	0.47	40	195.2	0.47

41	200.2	0.34		41	200.2	0.34
42	205.11	0.1		42	205.11	0.1
43	210.24	0.46		43	210.24	0.46
44	215.32	0.47		44	215.32	0.47
45	220.27	0.41		45	220.27	0.41
46	225.05	0.11		46	225.05	0.11
47	230.3	0.57		47	230.3	0.57
48	235.21	0.57		48	235.21	0.57
49	240.3	0.51		49	240.3	0.51
50	245.25	0.55		50	245.25	0.55
51	250.33	0.54		51	250.33	0.54
52	255.23	0.54		52	255.23	0.54
53	260.18	0.54		53	260.18	0.54
54	265.27	0.51		54	265.27	0.51
55	270.22	0.57		55	270.22	0.57
56	275.31	0.6		56	275.31	0.6
57	280.21	0.54		57	280.21	0.54
58	285.34	0.59		58	285.34	0.59
59	290.24	0.56		59	290.24	0.56
60	295.25	0.61		60	295.25	0.61
61	300.15	0.65		61	300.15	0.65
62	305.28	0.64		62	305.28	0.64
63	310.18	0.69		63	310.18	0.69
64	315.49	0.6		64	315.49	0.6
65	320.19	0.76		65	320.19	0.76
66	325.23	0.71		66	325.23	0.71
67	330.24	0.76		67	330.24	0.76
68	335.32	0.8		68	335.32	0.8
69	340.18	0.74		69	340.18	0.74
70	345.08	0.78		70	345.08	0.78
71	350.05	0.92		71	350.05	0.92
72	355.22	0.93		72	355.22	0.93
73	360.31	0.89				
74	365.71	0.93		74	365.71	0.93
75	370.31	0.95		75	370.31	0.95
76	375.07	1.04		76	375.07	1.04
77	380.16	1.05		77	380.16	1.05
78	385.24	1.08		78	385.24	1.08
79	390.06	1.13		79	390.06	1.13
80	395.05	1.1		80	395.05	1.1
81	400.07	0.87		81	400.07	0.87
82	404.36	0.98		82	404.36	0.98
83	408.81	1.01		83	408.81	1.01
84	412.39	1.16				
85	417.79	1.23		85	417.79	1.23
86	420.3	1.31		86	420.3	1.31
87	425.2	1.37		87	425.2	1.37
88	429.82	1.42		88	429.82	1.42
89	435.19	1.41		89	435.19	1.41
90	440.01	1.5		90	440.01	1.5
91	445.09	1.54		91	445.09	1.54
92	449.96	1.64		92	449.96	1.64
93	454.87	1.75		93	454.87	1.75
94	459.95	1.92		94	459.95	1.92
95	464.9	2.09		95	464.9	2.09
96	470.04	2.19		96	470.04	2.19
97	474.95	2.5		97	474.95	2.5
98	479.85	2.8		98	479.85	2.8
99	484.84	3.1		99	484.84	3.1
100	489.88	3.38		100	489.88	3.38
101	494.89	3.74		101	494.89	3.74
102	499.75	4.08		102	499.75	4.08
103	504.8	4.53		103	504.8	4.53
104	509.84	4.9		104	509.84	4.9
105	514.79	5.5		105	514.79	5.5
106	519.88	5.9		106	519.88	5.9
107	524.61	6.22		107	524.61	6.22
108	529.82	6.72		108	529.82	6.72
109	534.73	7.11		109	534.73	7.11
110	539.86	7.6		110	539.86	7.6

111	544.77	8.13		111	544.77	8.13
112	549.89	8.58		112	549.89	8.58
113	554.8	9.05		113	554.8	9.05
114	559.42	9.5		114	559.42	9.5
115	564.38	9.93		115	564.38	9.93
116	569.29	10.43		116	569.29	10.43
117	574.19	10.98		117	574.19	10.98

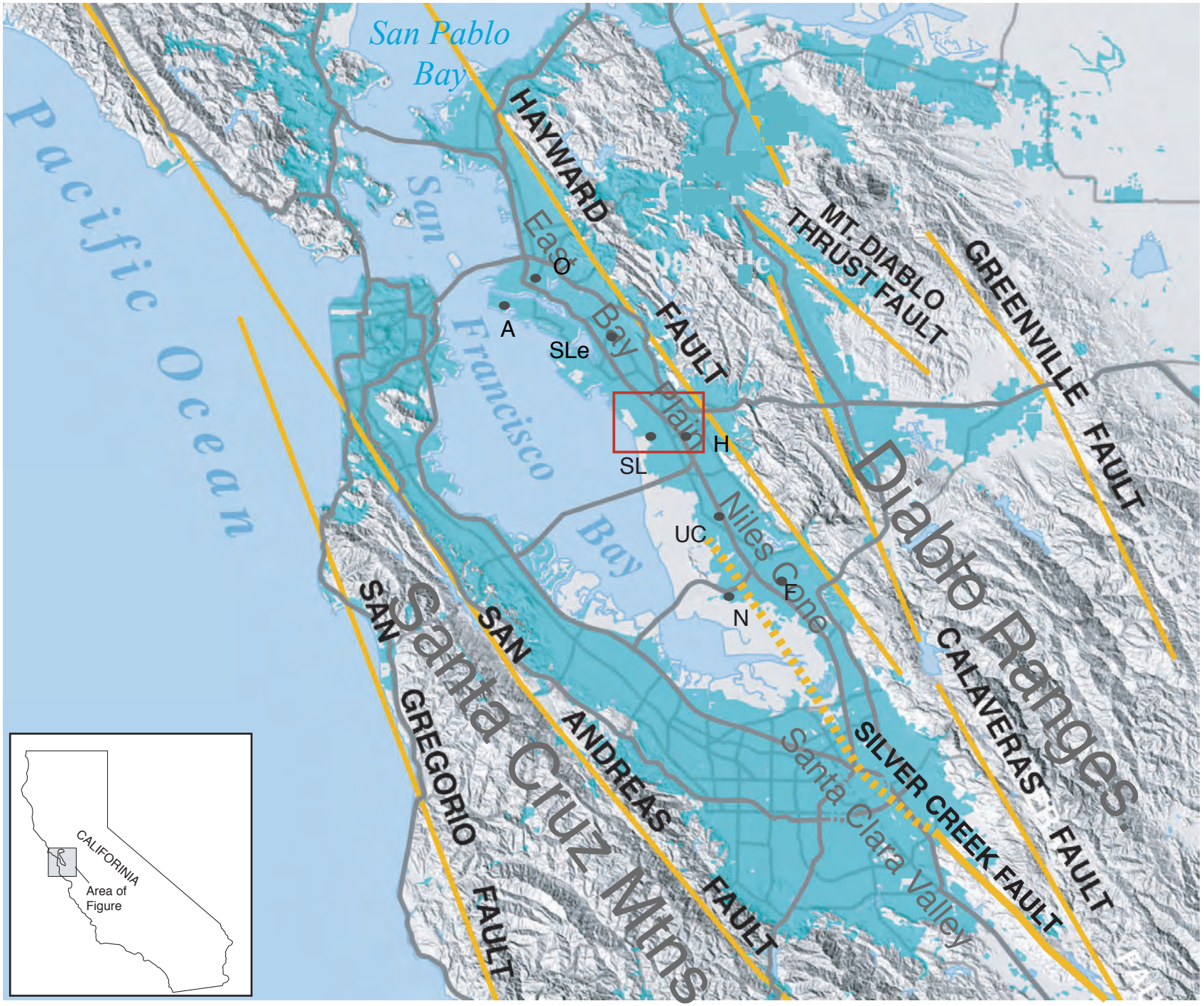
San Pablo Bay
Pacific Ocean
San Francisco Bay
East Bay Plain
HAYWARD FAULT
MT. DIABLO THRUST FAULT
GREENVILLE FAULT
CALAVERAS FAULT
SILVER CREEK FAULT
SAN ANDREAS FAULT
SAN GREGORIO FAULT
Diablo Ranges
Santa Cruz Mtns
Niles Cone
Santa Clara Valley
O
A
SLe
H
SL
UC
F
N
CALIFORNIA
Area of Figure

Fig 1

East Bay Plain Seismic Transect

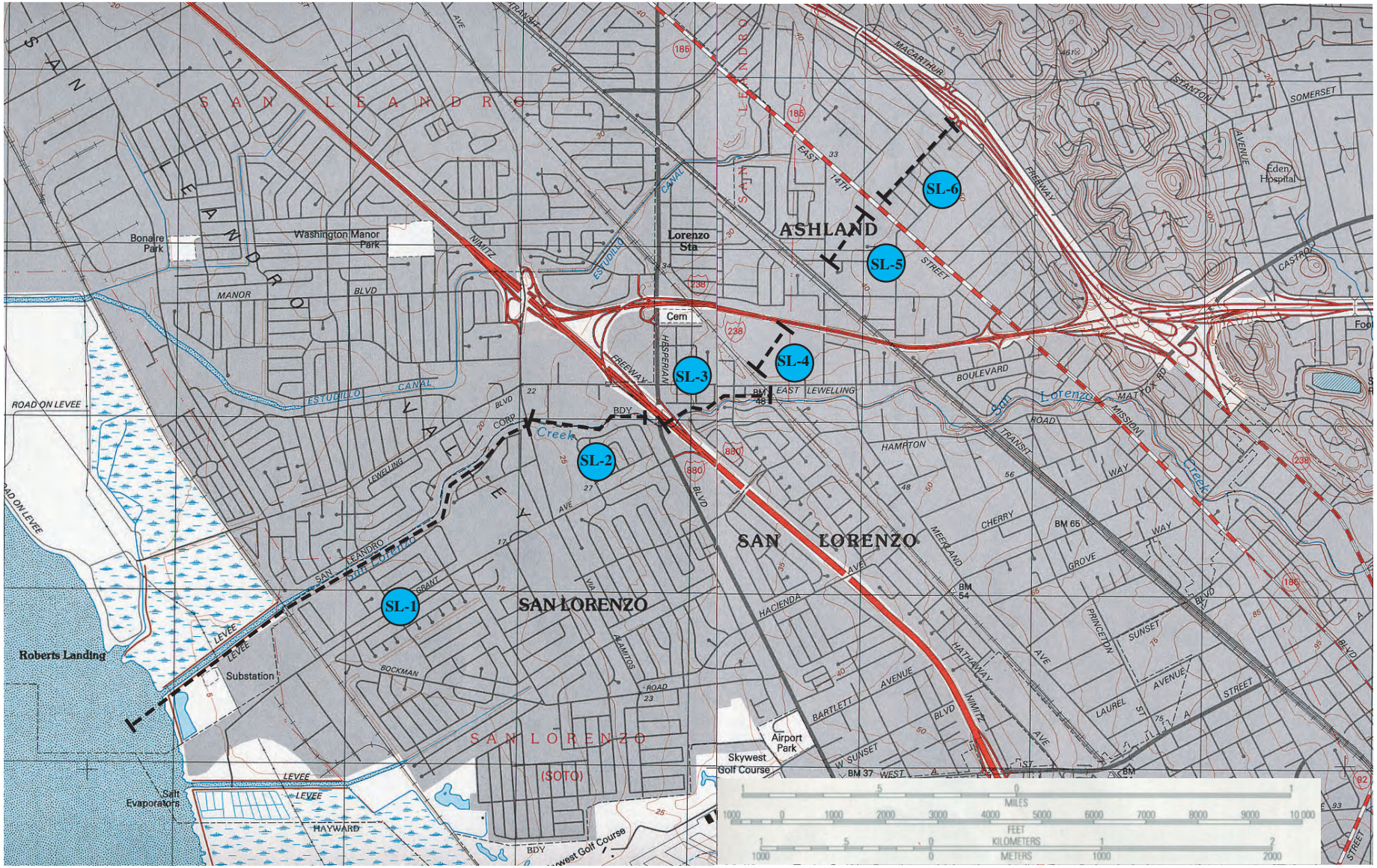

Fig. 2

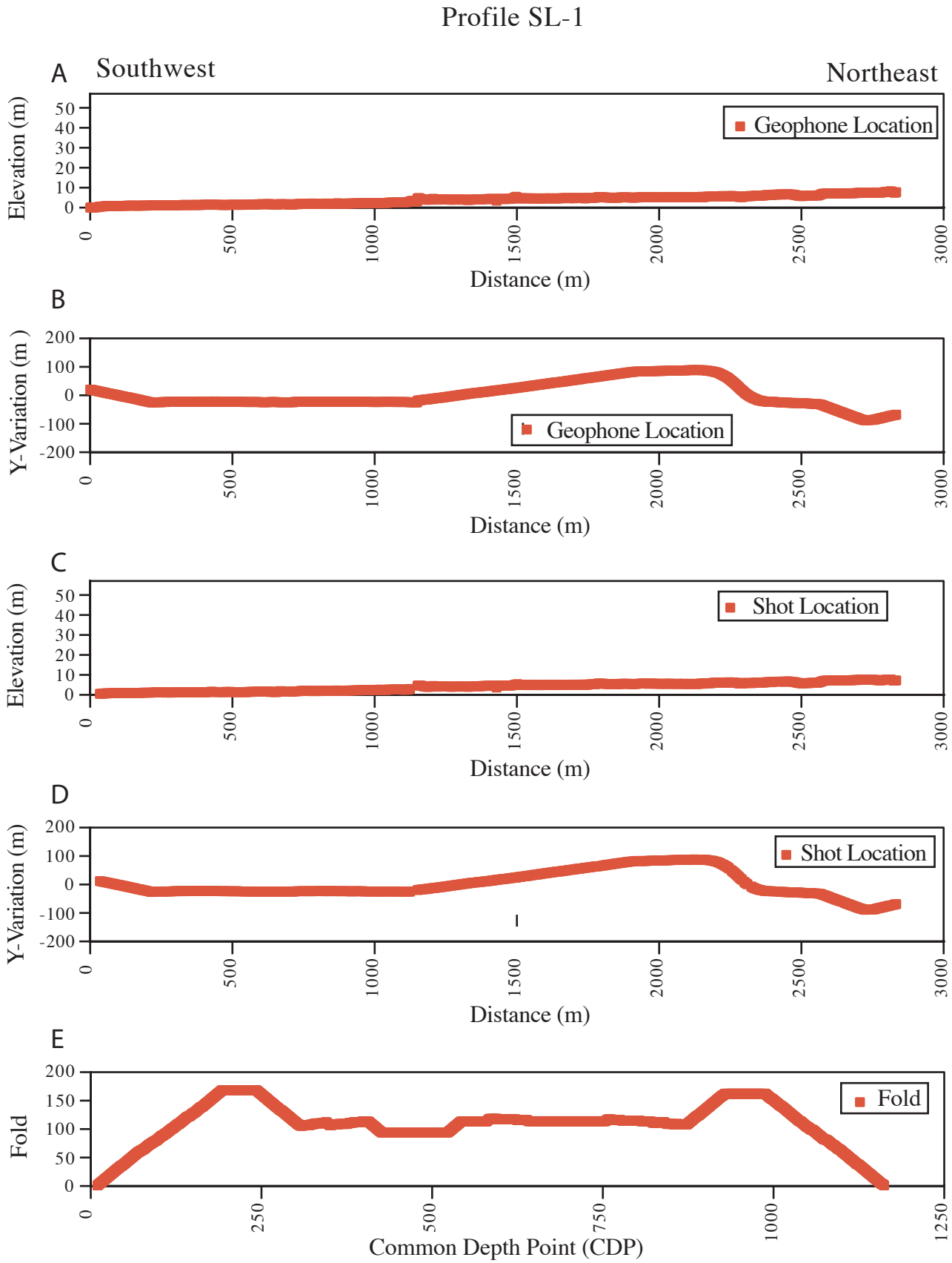
Profile SL-1
A
Southwest
Northeast
Elevation (m)
50
40
30
20
10
0
Geophone Location
0
500
1000
1500
2000
2500
3000
Distance (m)
B
Y-Variation (m)
200
100
0
-100
-200
Geophone Location
Distance (m)
C
Elevation (m)
Shot Location
Distance (m)
D
Y-Variation (m)
Shot Location
Distance (m)
E
Fold
200
150
100
50
0
Fold
0
250
500
750
1000
1250
Common Depth Point (CDP)

Fig. 3

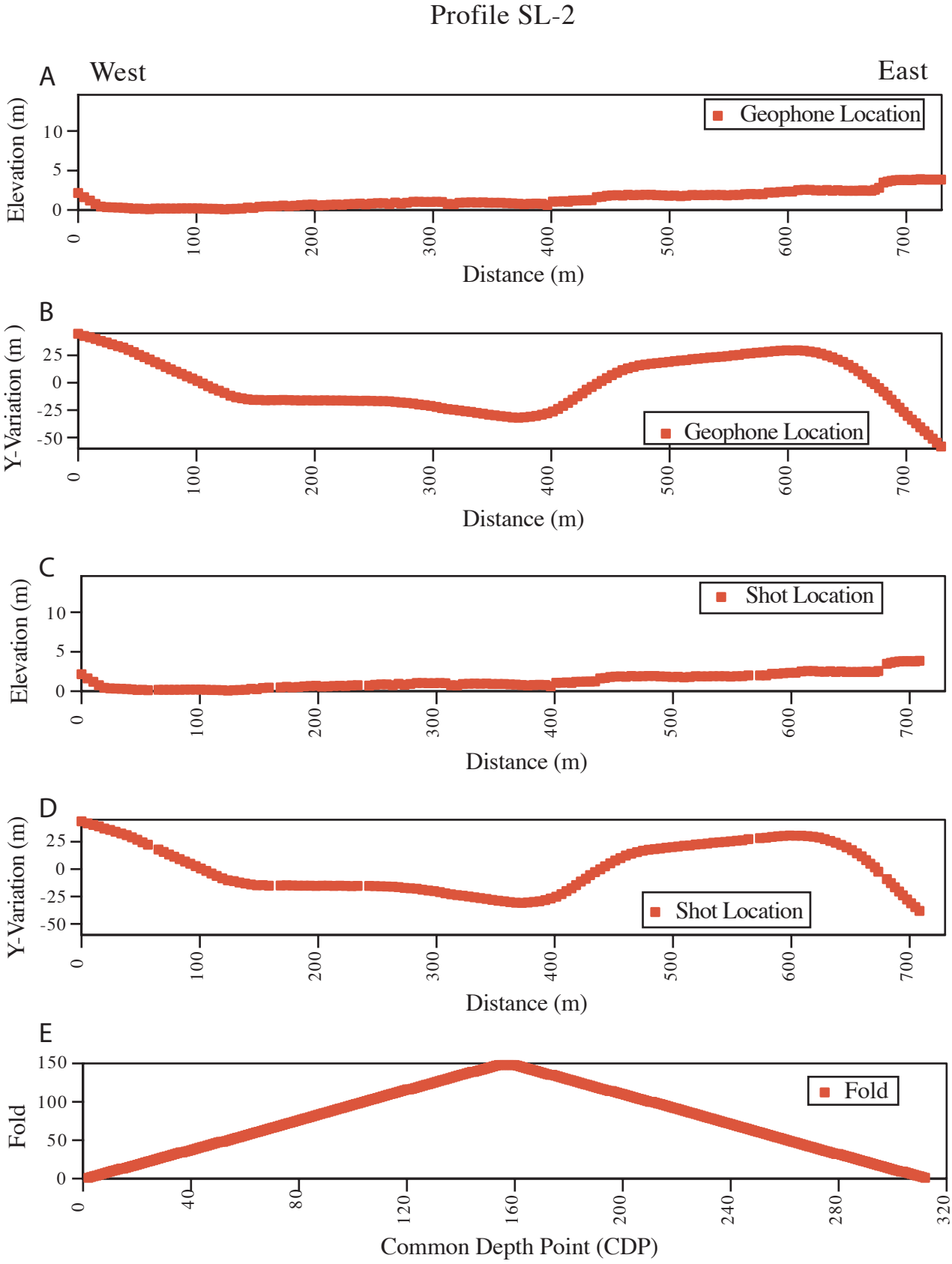
Profile SL-2
A
West
East
Elevation (m)
10
5
0
Geophone Location
0
100
200
300
400
500
600
700
Distance (m)
B
Y-Variation (m)
25
0
-25
-50
Geophone Location
Distance (m)
C
Elevation (m)
Shot Location
Distance (m)
D
Y-Variation (m)
Shot Location
Distance (m)
E
Fold
150
100
50
0
Fold
0
40
80
120
160
200
240
280
320
Common Depth Point (CDP)

Fig. 4

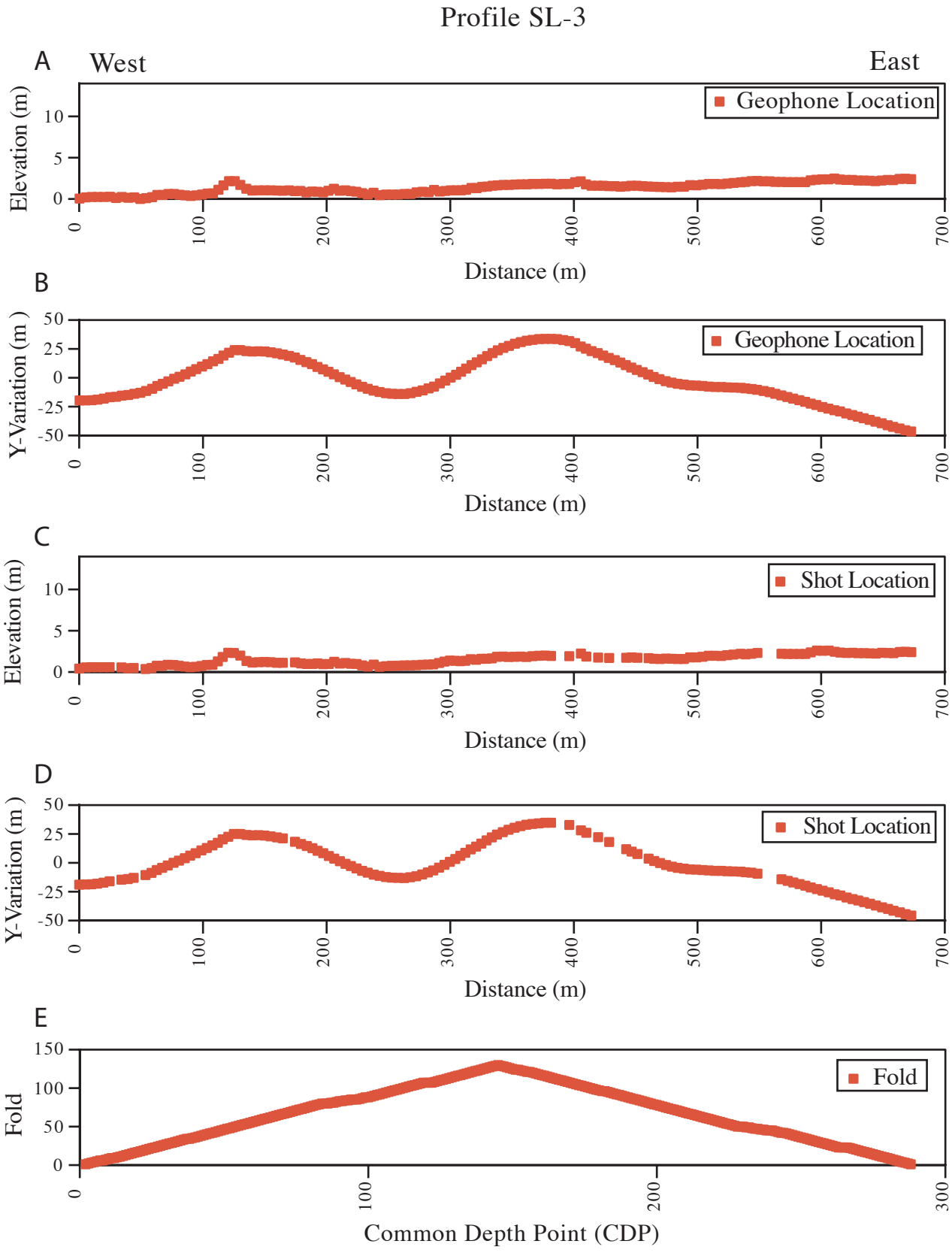
Profile SL-3
A
West
East
Elevation (m)
10
5
0
Geophone Location
0
100
200
300
400
500
600
700
Distance (m)
B
Y-Variation (m)
50
25
0
-25
-50
Geophone Location
Distance (m)
C
Elevation (m)
Shot Location
Distance (m)
D
Y-Variation (m)
Shot Location
Distance (m)
E
Fold
150
100
50
0
Fold
0
100
200
300
Common Depth Point (CDP)

Fig. 5

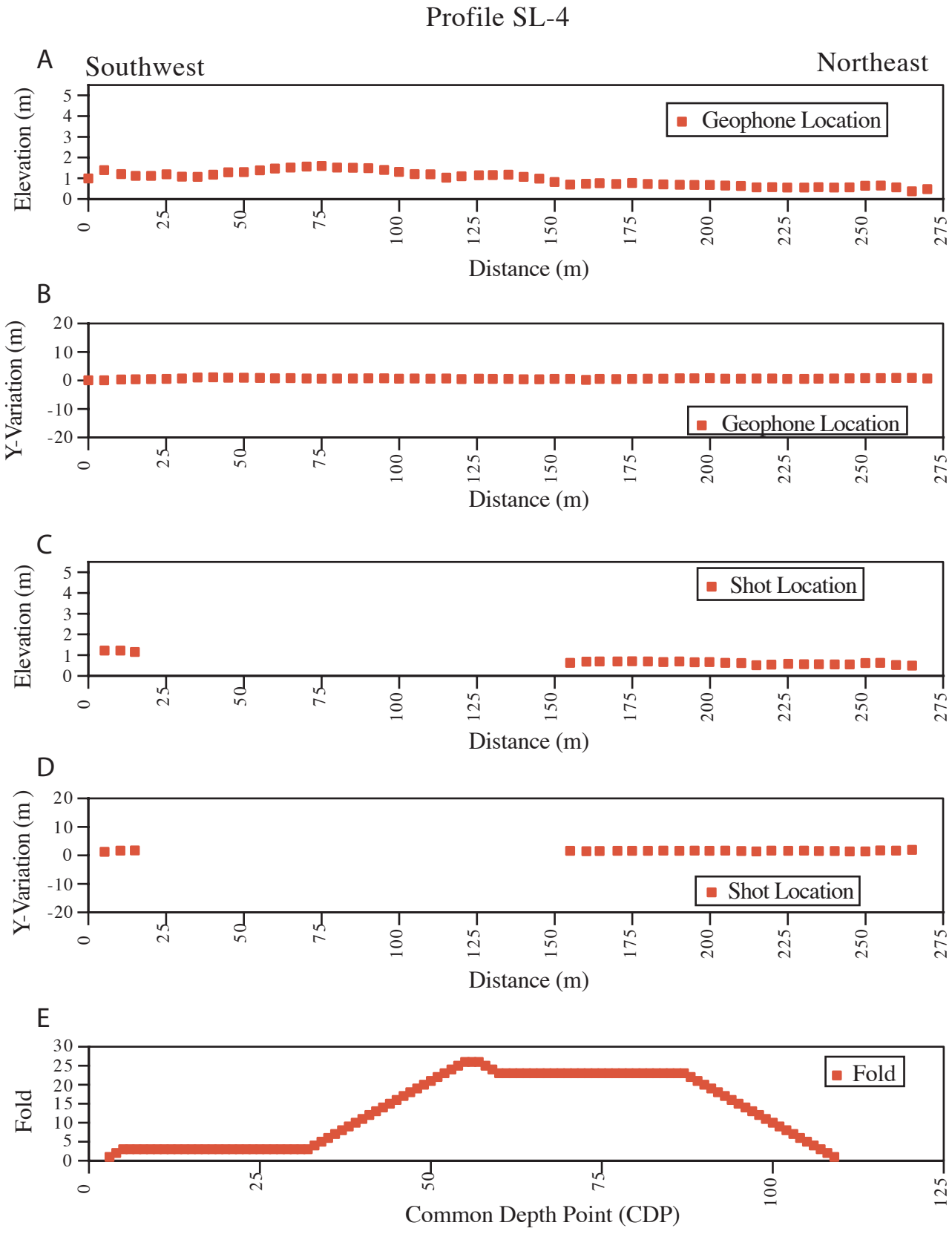
Profile SL-4
A
Southwest
Northeast
Elevation (m)
Geophone Location
Distance (m)
B
Y-Variation (m)
Geophone Location
Distance (m)
C
Elevation (m)
Shot Location
Distance (m)
D
Y-Variation (m)
Shot Location
Distance (m)
E
Fold
Fold
Common Depth Point (CDP)

Fig. 6

Profile SL-5

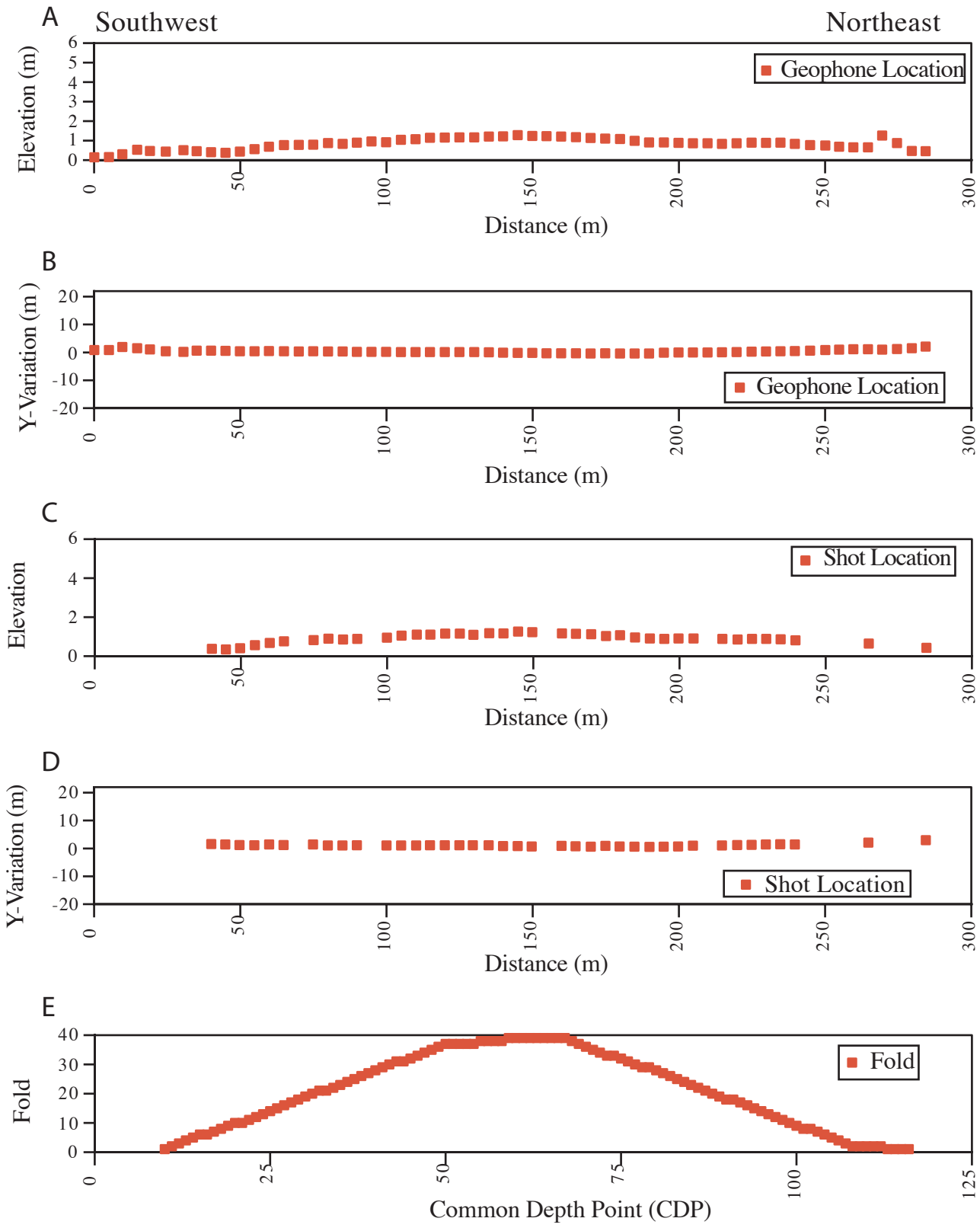

Fig. 7

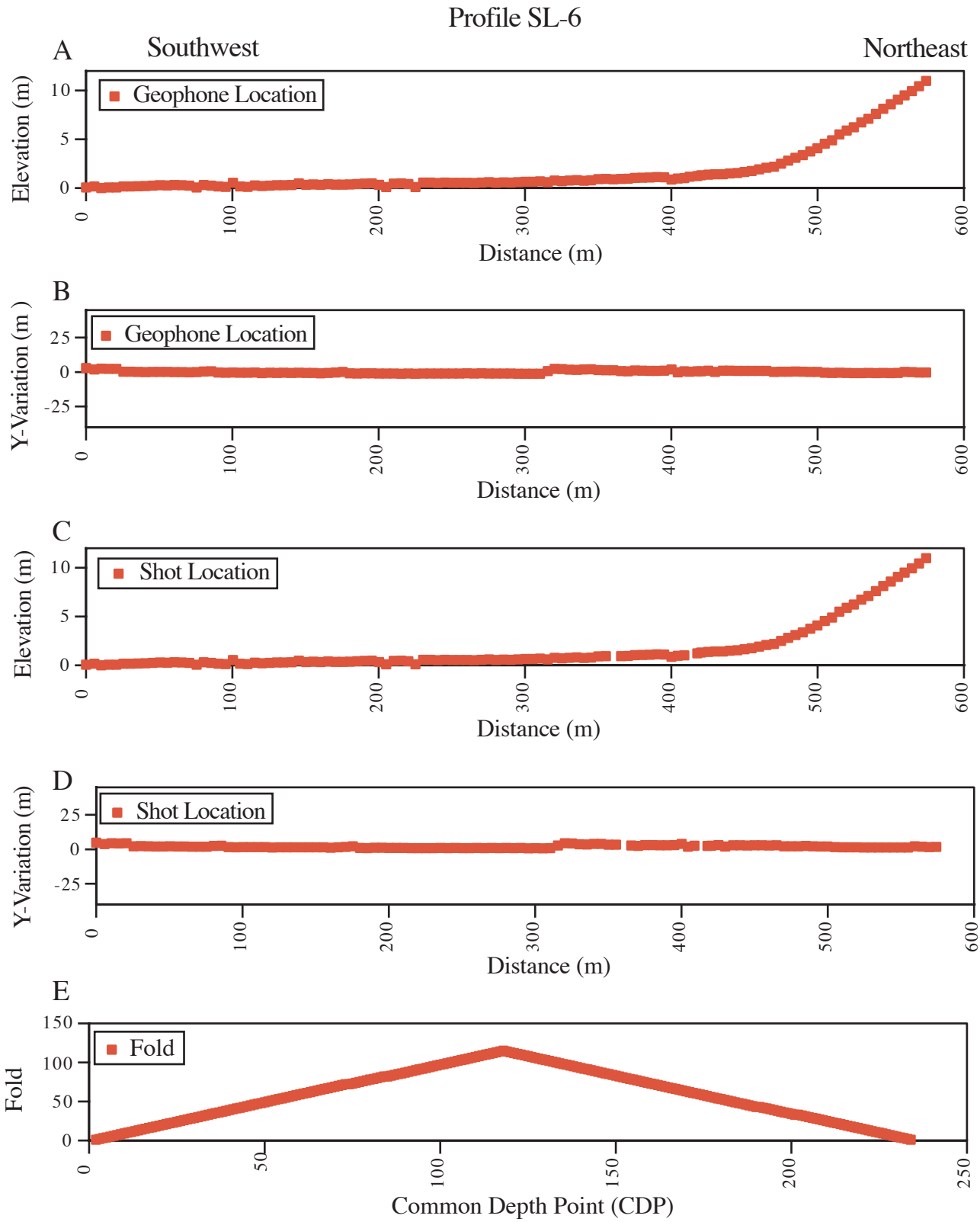
Profile SL-6
A
Southwest
Northeast
Geophone Location
Elevation (m)
Distance (m)
B
Geophone Location
Y-Variation (m)
Distance (m)
C
Shot Location
Elevation (m)
Distance (m)
D
Shot Location
Y-Variation (m)
Distance (m)
E
Fold
Fold
Common Depth Point (CDP)

Fig. 8

Figure 9 is an oversize illustration and is a separate file.

View Figure 9 as a 68" x 13" file (of2006-1084_fig09.pdf; 2.6 MB)

Figure 10 is an oversize illustration and is a separate file.

View Figure 10 as a 46" x 20" file (of2006-1084_fig10.pdf; 14.3 MB)

Figure 11 is an oversize illustration and is a separate file.

View Figure 11 as a 68" x 16" file (of2006-1084_fig11.pdf; 9.3 MB)

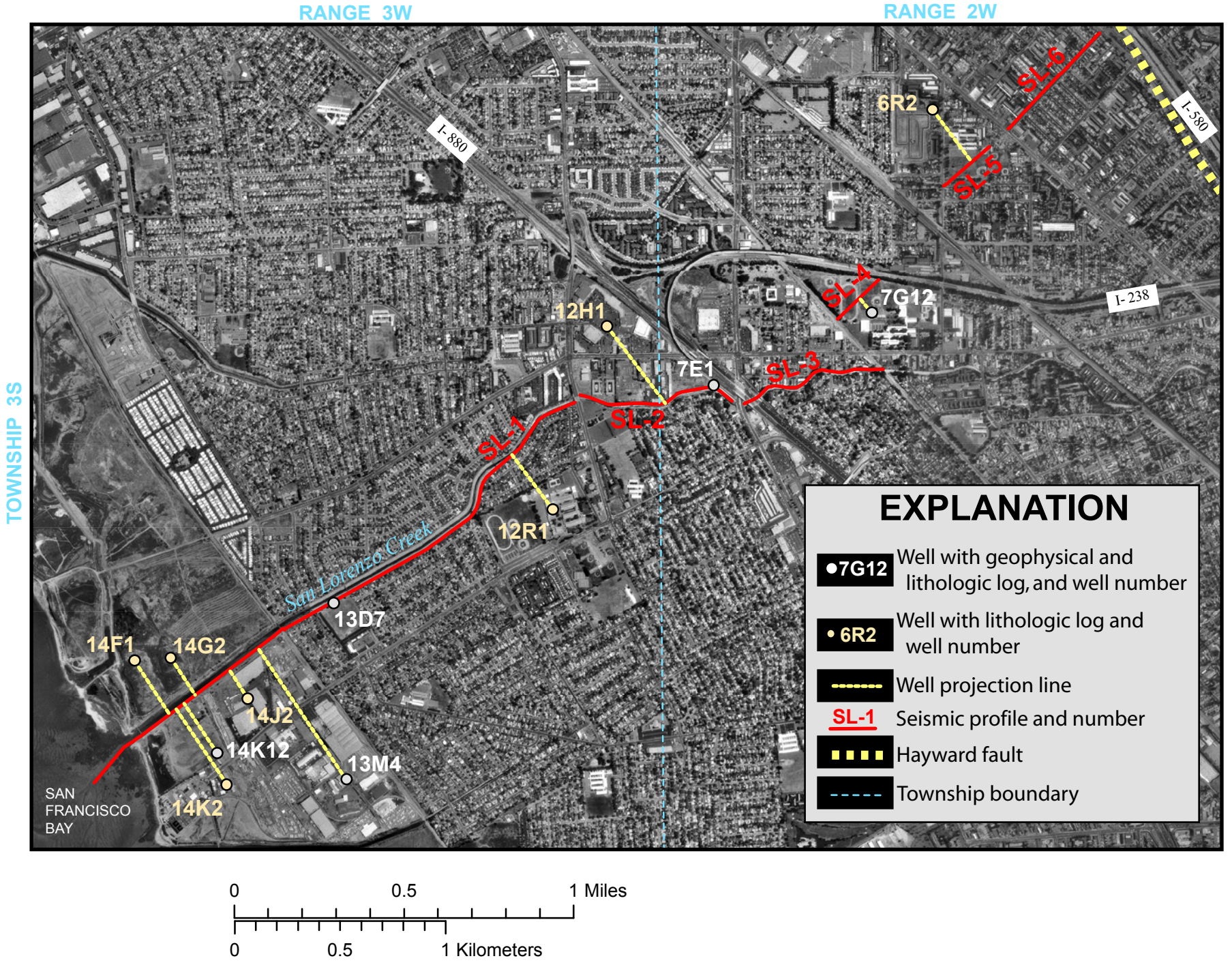
RANGE 3W
RANGE 2W
TOWNSHIP 3S
I-880
I-580
I-238
6R2
SL-5
SL-6
7G12
SL-4
12H1
7E1
SL-3
SL-2
SL-1
12R1
San Lorenzo Creek
13D7
14F1
14G2
14J2
14K12
13M4
14K2
SAN FRANCISCO BAY
EXPLANATION
7G12 Well with geophysical and lithologic log, and well number
6R2 Well with lithologic log and well number
Well projection line
SL-1 Seismic profile and number
Hayward fault
Township boundary
0 0.5 1 Miles
0 0.5 1 Kilometers

Figure 12.

Figure 13 is an oversize illustration and is a separate file.

View Figure 13 as a 70" x 16" file (of2006-1084_fig13.pdf; 14.3 MB)

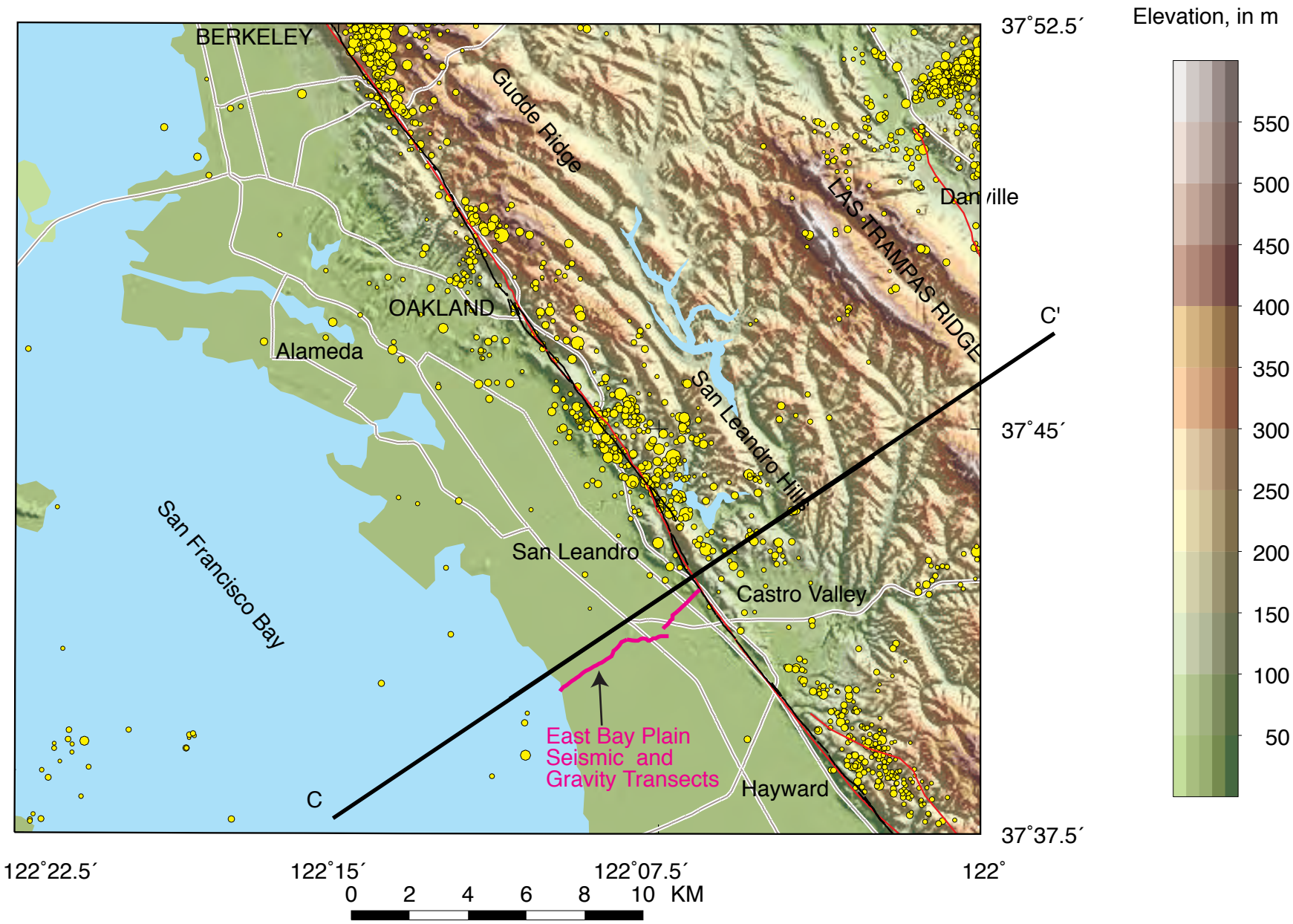
BERKELEY
Gudde Ridge
LAS TRAMPAS RIDGE
Dan ville
OAKLAND
Alameda
San Leandro Hills
San Francisco Bay
San Leandro
Castro Valley
East Bay Plain
Seismic and
Gravity Transects
Hayward
C
C'
37˚52.5´
37˚45´
37˚37.5´
122˚22.5´
122˚15´
122˚07.5´
122˚
0 2 4 6 8 10 KM
Elevation, in m
550
500
450
400
350
300
250
200
150
100
50

Fig. 14

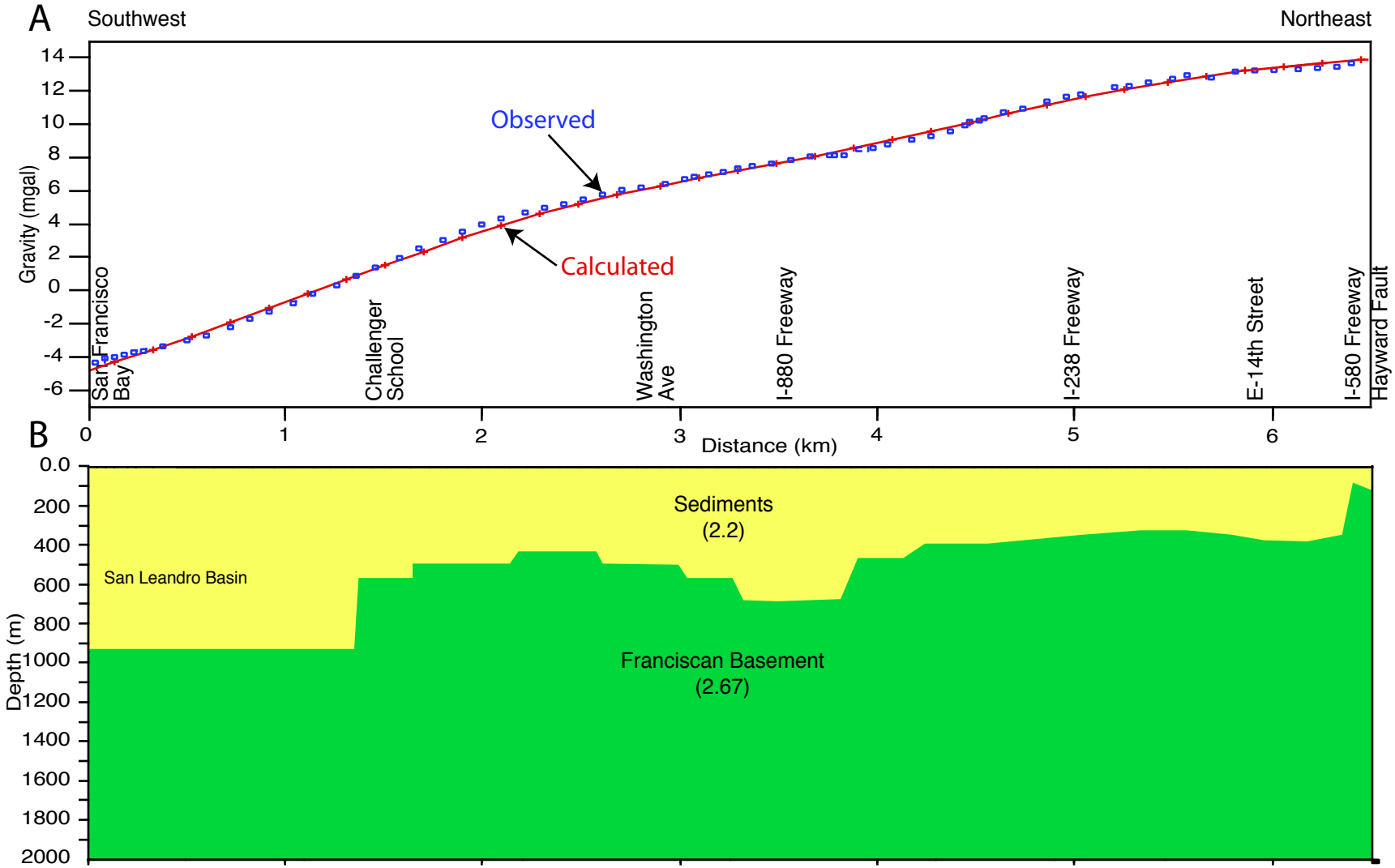
A
Southwest
Northeast
Gravity (mgal)
14
12
10
8
6
4
2
0
-2
-4
-6
Observed
Calculated
San Francisco Bay
Challenger School
Washington Ave
I-880 Freeway
I-238 Freeway
E-14th Street
I-580 Freeway
Hayward Fault
0
1
2
3
4
5
6
Distance (km)
B
Depth (m)
0.0
200
400
600
800
1000
1200
1400
1600
1800
2000
Sediments
(2.2)
San Leandro Basin
Franciscan Basement
(2.67)

Fig. 15

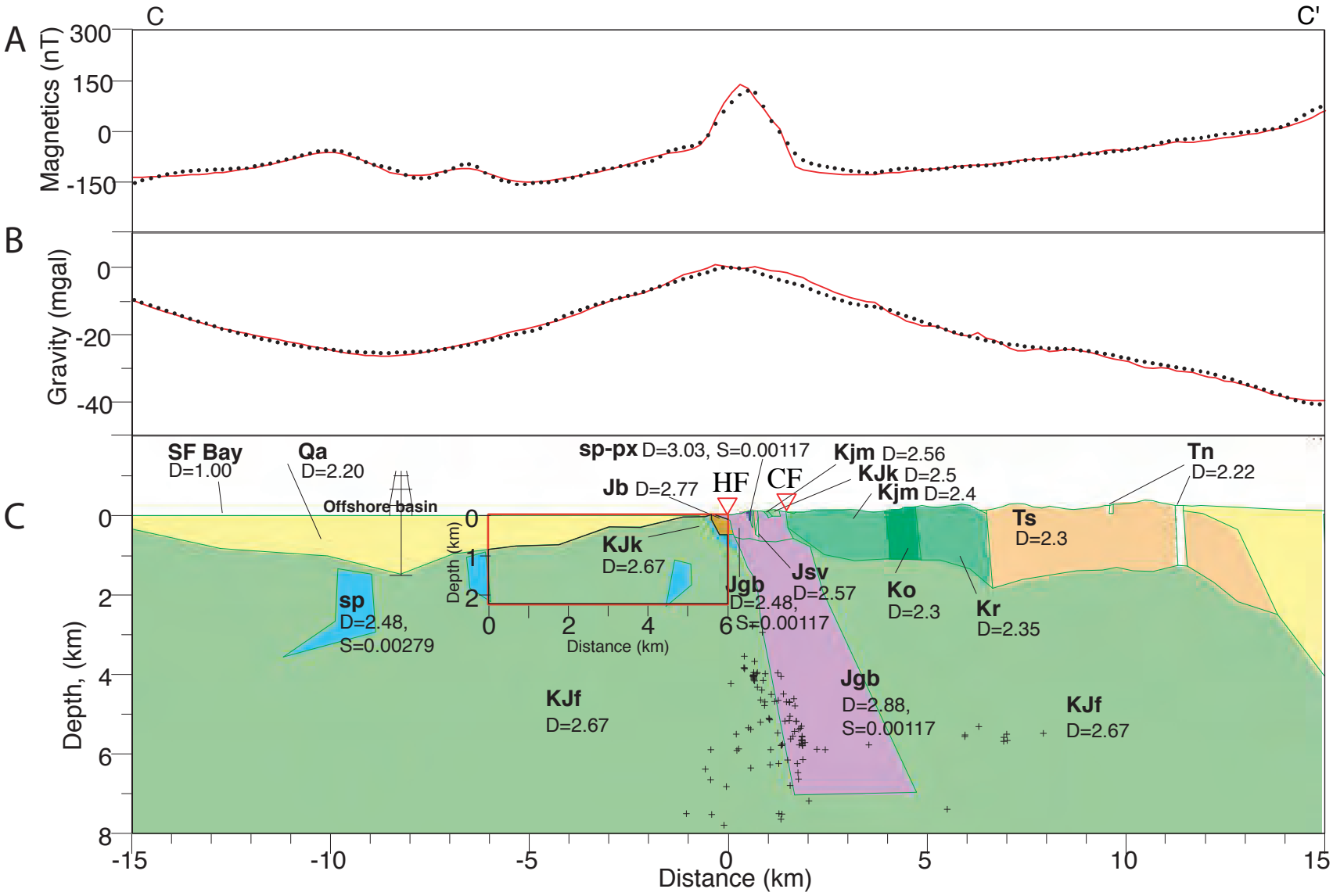
A
B
C
C
C'
Magnetics (nT)
300
150
0
-150
Gravity (mgal)
0
-20
-40
SF Bay
D=1.00
Qa
D=2.20
Offshore basin
sp
D=2.48,
S=0.00279
sp-px D=3.03, S=0.00117
Jb D=2.77
HF
CF
Kjm D=2.56
KJk D=2.5
Kjm D=2.4
Tn
D=2.22
Ts
D=2.3
KJk
D=2.67
Jsv
D=2.57
Jgb
D=2.48,
S=0.00117
Ko
D=2.3
Kr
D=2.35
KJf
D=2.67
Jgb
D=2.88,
S=0.00117
KJf
D=2.67
Depth (km)
Distance (km)
Depth, (km)
Distance (km)
-15
-10
-5
0
5
10
15
0
2
4
6
8

Fig. 16

Figure 17a is an oversize illustration and is a separate file.

View Figure 17a as a 46" x 20" file (of2006-1084_fig17a.pdf; 35.1 MB)

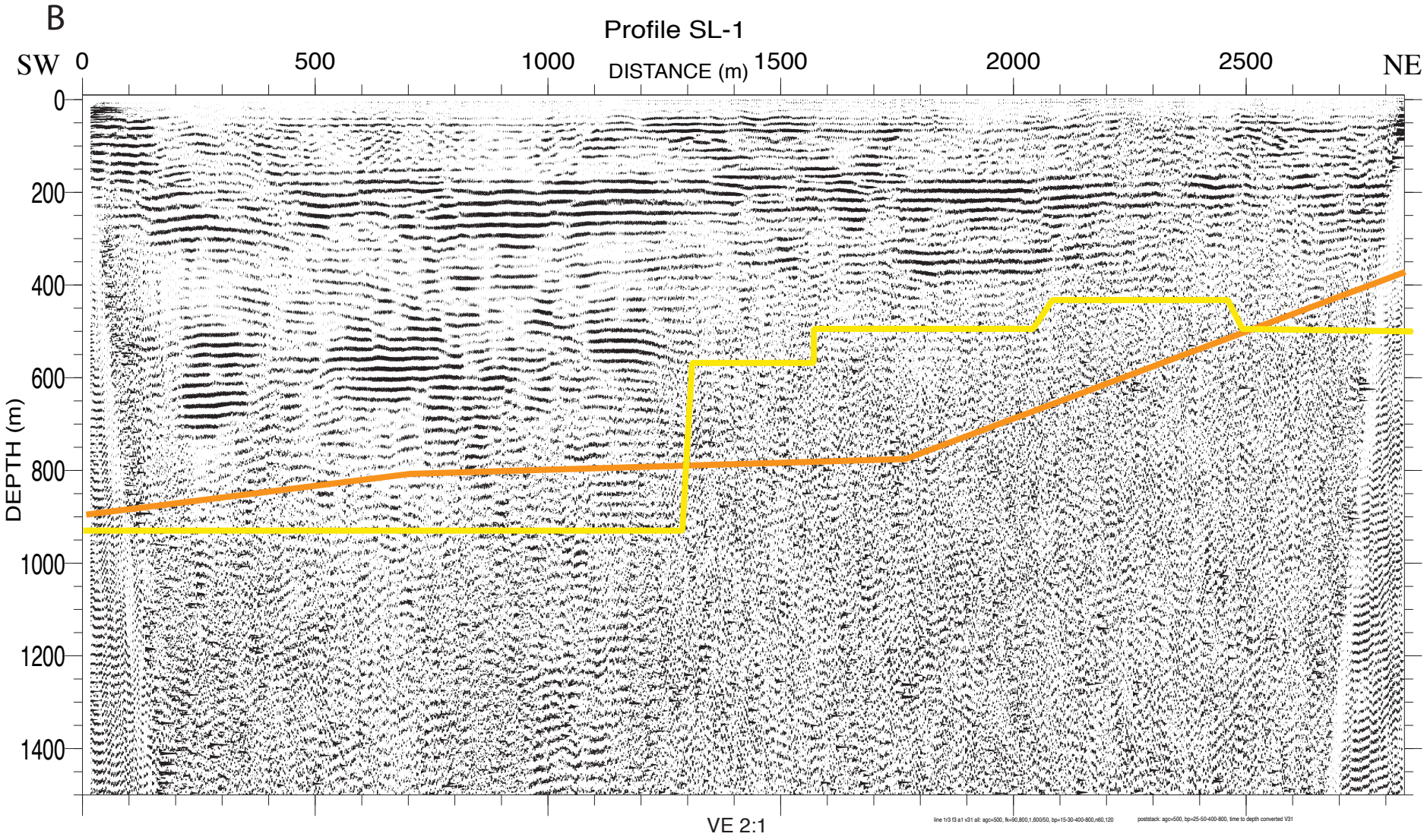
B
Profile SL-1
SW
NE
DISTANCE (m)
0
500
1000
1500
2000
2500
DEPTH (m)
0
200
400
600
800
1000
1200
1400
VE 2:1

Fig. 17b

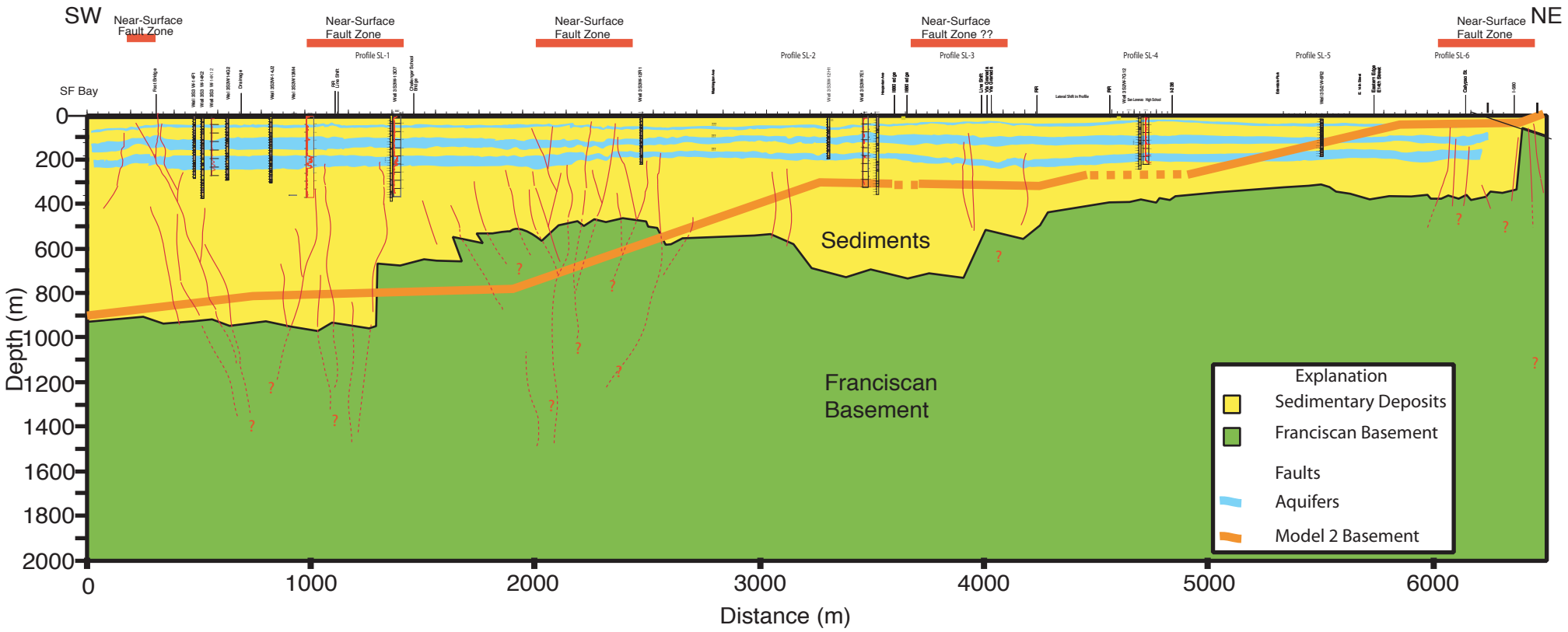
SW
NE
Near-Surface Fault Zone
Near-Surface Fault Zone
Near-Surface Fault Zone
Near-Surface Fault Zone ??
Near-Surface Fault Zone
Profile SL-1
Profile SL-2
Profile SL-3
Profile SL-4
Profile SL-5
Profile SL-6
SF Bay
Sediments
Franciscan Basement
Explanation
Sedimentary Deposits
Franciscan Basement
Faults
Aquifers
Model 2 Basement
Depth (m)
0
200
400
600
800
1000
1200
1400
1600
1800
2000
0
1000
2000
3000
4000
5000
6000
Distance (m)

Fig.18

Figure 19 is an oversize illustration and is a separate file.

View Figure 19 as a 70" x 17" file (of2006-1084_fig19.pdf; 15.8 MB)

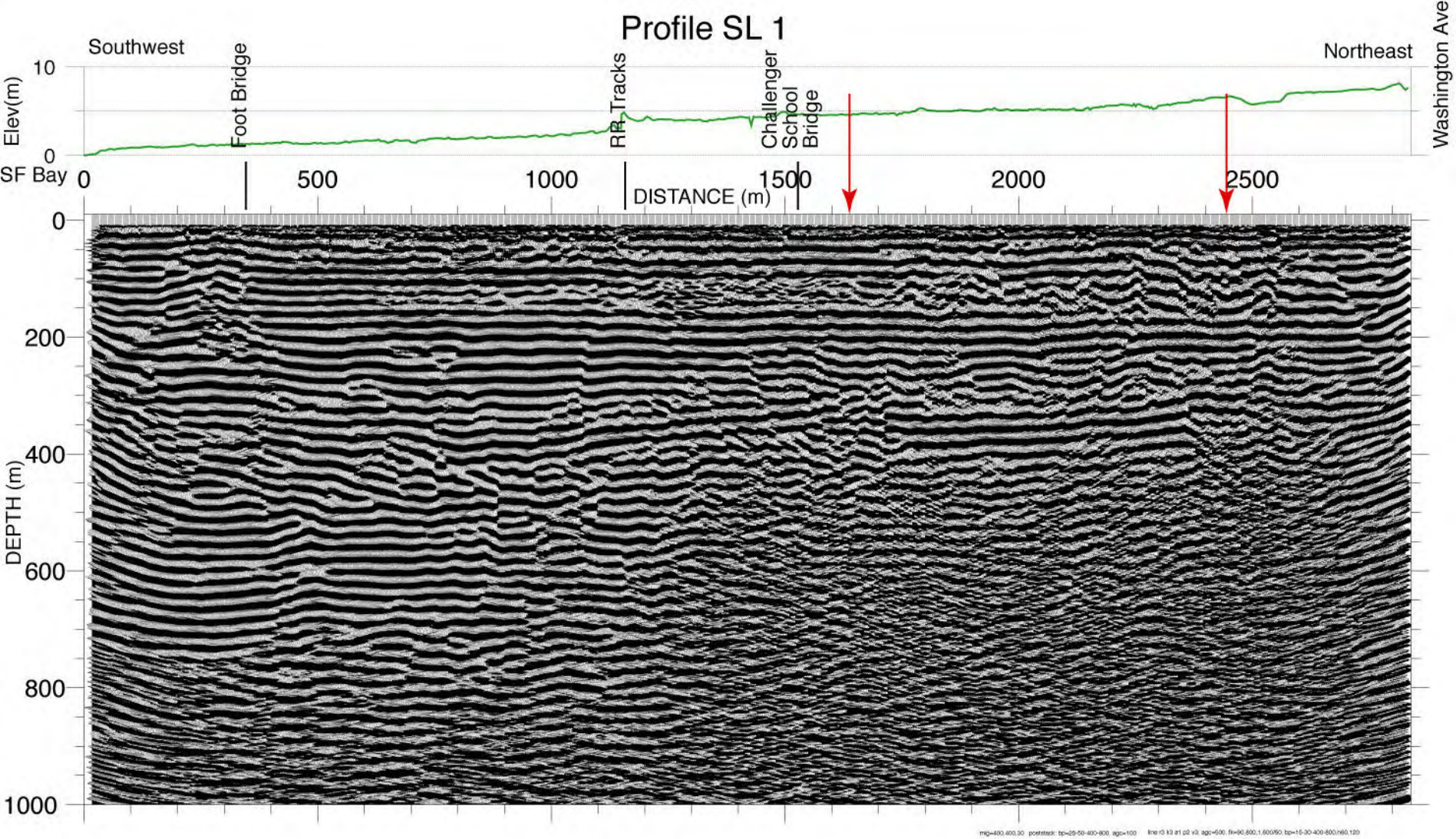
Profile SL 1
Southwest
Northeast
Elev(m)
10
0
SF Bay
Foot Bridge
RR Tracks
Challenger School Bridge
Washington Ave
0
500
1000
1500
2000
2500
DISTANCE (m)
DEPTH (m)
0
200
400
600
800
1000

Fig. 20

Figure 21 is an oversize illustration and is a separate file.

View Figure 21 as a 50" x 20" file (of2006-1084_fig21.pdf; 16 MB)

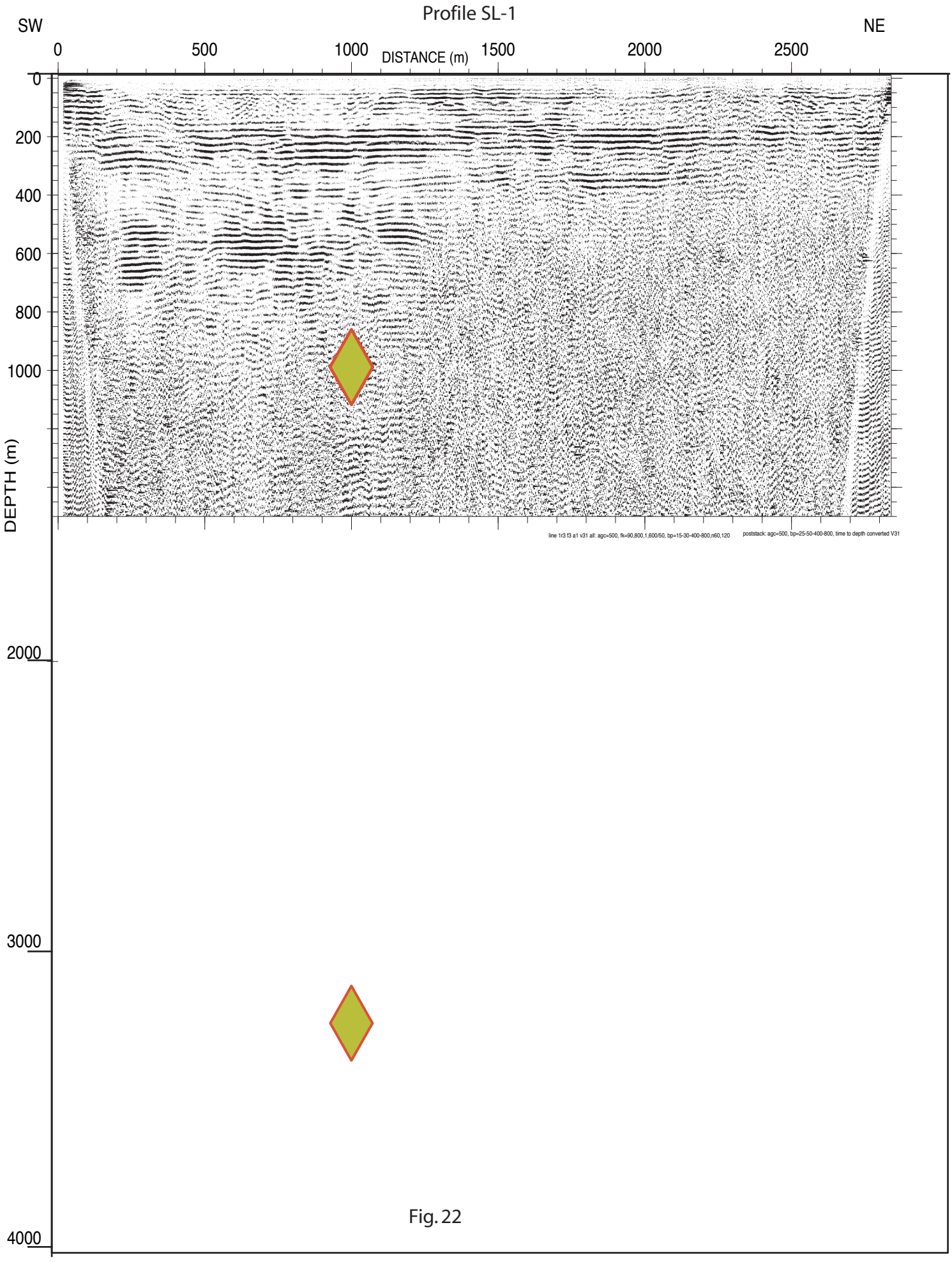
Profile SL-1
SW
NE
0
500
1000
1500
2000
2500
DISTANCE (m)
0
200
400
600
800
1000
2000
3000
4000
DEPTH (m)
line 1r3 f3 a1 v31 all: agc=500, fk=90,800,1,600/50, bp=15-30-400-800,n60,120
poststack: agc=500, bp=25-50-400-800, time to depth converted V31

Fig. 22